

Physics Opportunities at $\mu^+\mu^-$ Higgs Factories *

C. Blöchliger^a, M. Carena^b, J. Ellis^c, H. Fraas^a, F. Franke^a, D. Garcia^c, S. Heinemeyer^d, S. Kraml^{c,e}, G. Moortgat-Pick^f, W. Murray^g, F. von der Pahlen^a, A. Pilaftsis^{a,h}, C.E.M. Wagner^{i,j} and G. Weiglein^{c,k}

a Inst. f. Theoretische Physik und Astrophysik, Univ. Würzburg, D-97074 Würzburg, Germany

b Fermilab, P.O. Box 500, Batavia IL 60510, U.S.A.

c Theory Division, CERN, CH-1211 Geneva 23, Switzerland

d HET, Physics Department, Brookhaven Natl. Lab., Upton, NY 11973 USA

e Inst. f. Hochenergiephysik, Österr. Akademie d. Wissenschaften, A-1050 Vienna, Austria

f DESY, Deutsches Elektronen-Synchrotron, D-22603 Hamburg, Germany

g RAL, Chilton, Didcot, Oxon., OX11 0QX, UK

h Department of Physics and Astronomy, Univ. of Manchester, Manchester M13 9PL, U.K.

i High Energy Physics Division, Argonne National Lab., Argonne IL 60439, U.S.A.

j Enrico Fermi Institute, University of Chicago, 5640 Ellis Ave., Chicago IL 60637, U.S.A.

k Institute for Particle Physics Phenomenology, University of Durham, Durham DH1 3LR, UK

Abstract

We update theoretical studies of the physics opportunities presented by $\mu^+\mu^-$ Higgs factories. Interesting measurements of the Standard Model Higgs decays into $b\bar{b}$, $\tau^+\tau^-$ and WW^* may be possible if the Higgs mass is less than about 160 GeV, as preferred by the precision electroweak data, the mass range being extended by varying appropriately the beam energy resolution. A suitable value of the beam energy resolution would also enable the uncertainty in the b -quark mass to be minimized, facilitating measurements of parameters in the MSSM at such a first $\mu^+\mu^-$ Higgs factory. These measurements would be sensitive to radiative corrections to the Higgs-fermion-antifermion decay vertices, which may violate CP. Radiative corrections in the MSSM may also induce CP violation in Higgs-mass mixing, which can be probed via various asymmetries measurable using polarized $\mu^+\mu^-$ beams. In addition, Higgs-chargino couplings may be probed at a second $\mu^+\mu^-$ Higgs factory.

1 Introduction

Muon colliders produce Higgs bosons directly via $\mu^+\mu^-$ annihilation in the s -channel, unaccompanied by spectator particles. If the electroweak symmetry is broken via the Higgs mechanism, hadron machines, such as the Tevatron collider [1] and the LHC [2], will presumably discover at least one Higgs boson, but in an experimental environment contaminated by important backgrounds and accompanied by many other particles. An e^+e^- linear collider (LC) [3, 4, 5] would complement the hadron colliders by providing precise studies of the Higgs boson in a clean environment. However, the dominant production mechanisms create Higgs bosons in association with other particles, such as a Z^0 , two neutrinos or an e^+e^- pair. Moreover, the peak cross section for a $\mu^+\mu^-$ collider to produce a Higgs of 115 GeV is around 60 pb, which can be compared with around 0.14 pb for an e^+e^- collider operating at 350 GeV.

*Report of the Higgs factory working group of the ECFA-CERN study on Neutrino Factory & Muon Storage Rings at CERN.

The potential of $\mu^+\mu^-$ colliders for investigations of the Higgs system is very exciting, and has been the subject of much work, see, e.g., [6, 7, 8]. However, if the study of an s -channel resonance is to be pursued experimentally, the event rate must be sufficiently large. In the case of a Standard Model (SM) Higgs boson H , this means that the mass must be somewhat less than twice M_W , otherwise the large width reduces the peak cross section. This condition need not apply to more complicated Higgs systems, for instance the heavier neutral Higgses of supersymmetry.

Since a $\mu^+\mu^-$ collider is able to work near optimally over only a limited range of centre-of-mass energies, knowledge of the Higgs mass is crucial in designing such a machine. A combined fit to precision electroweak observables yields an indirect estimate for the SM Higgs boson mass of

$$m_H = 88^{+53}_{-35} \text{ GeV} . \quad (1.1)$$

with a one-sided 95% confidence-level upper limit of 196 GeV [9], including theoretical uncertainties. These numbers are increased by about 20 GeV if one uses the estimate [10] of the effective value of α_{em} at the Z^0 peak. The range (1.1) should be compared with the lower limit from direct searches of 114.1 GeV [11], and suggests that the most probable value for the Higgs mass is not much greater than this lower limit [12], as seen in Fig. 1. The analysis leading to Fig. 1 is valid within the Standard Model, or any new physics extension of it in which the new physics effects decouple from the precision electroweak observables, as occurs for example in minimal supersymmetric extensions of the Standard Model, when all supersymmetric particle masses are above the weak scale.

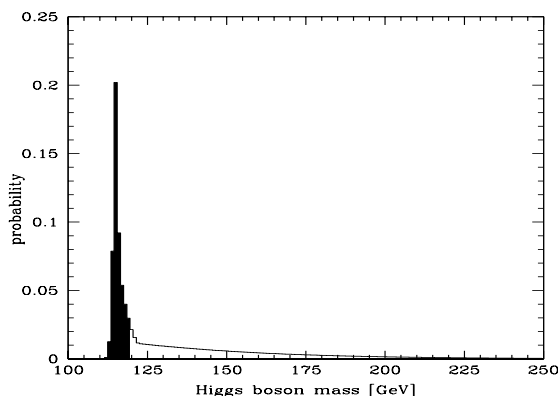


Fig. 1: Probability distribution for the mass of the SM Higgs boson, estimated [12] by combining the available indirect information with the LEP direct lower limit [11]. The shaded region represents 50% of the probability distribution.

In fact, the 2000 run of the LEP collider yielded a 2.1σ excess in the search for the SM Higgs boson, with a preferred mass of [11]

$$m_H = 115.6^{+1.4}_{-1.1} \text{ GeV} . \quad (1.2)$$

The excess seen is consistent with the expectations from such a signal: the most significant candidate events have been seen in the $H \rightarrow \bar{b}b$ decay mode, with $Z^0 \rightarrow \bar{q}q$, and the production cross section is quite compatible with that expected for a SM Higgs boson. The mass (1.2) is highly consistent with the range (1.1). Moreover, both are also highly compatible with the minimal supersymmetric extension of the Standard Model (MSSM), which predicts the existence of a light Higgs boson weighing less than about 130 GeV [14]. If the observation (1.2) were to be confirmed, it would provide an excellent opportunity for a $\mu^+\mu^-$ collider Higgs factory. As was outlined in [7], the

measurement of the $H \rightarrow \bar{b}b$ decay mode for a mass around 100 GeV suffers from excessive background if m_H is close to the Z peak, and from the rapidly-increasing Higgs width, and therefore reduced on-peak cross section, as m_H increases toward the W^+W^- threshold. The optimal Higgs mass identified in [7] was in fact 115 GeV.

In the coming years, first the Tevatron collider [1] and subsequently the LHC [2] will have opportunities to discover the SM Higgs boson. In the case of the (constrained) MSSM, it has been shown that the prospects for the lightest Higgs boson are nearly as good as for the SM [15]. One may expect to measure the mass of the SM or MSSM Higgs boson at the hadron colliders with a precision better than 1 GeV. Detailed follow-up measurements would then be possible with an e^+e^- linear collider [3, 4, 5]. Unfortunately, the existence of a Higgs boson weighing 115 GeV will probably not be clarified by the Tevatron collider or the LHC for several more years.

On the other hand, much work is still required before the feasibility of a $\mu^+\mu^-$ collider can be demonstrated. We recall that the muon collection and storage facility foreseen for a $\mu^+\mu^-$ collider has many parameters in common with those required for a neutrino factory [7], whose storage ring requires 10^{14} muons per second to be injected with a preferred energy of 50 GeV. This energy is close to that required for a first-generation $\mu^+\mu^-$ collider. However, a $\mu^+\mu^-$ collider would need about an order of magnitude more muons than are foreseen in the neutrino factory, and it is not yet clear what combination of higher-efficiency beam preparation and increased proton power will be the most effective way to achieve this. Moreover, the normalised emittance envisaged for a neutrino factory is 1.67 mm.rad, whereas 0.2 mm.rad is anticipated in $\mu^+\mu^-$ collider designs [16]. Thus, considerably more beam cooling would be required for a $\mu^+\mu^-$ collider. We recall also that the bunch structure foreseen for a neutrino factory, namely a train of 140 bunches injected at 75 Hz, would need to be modified. The luminosity of a collider scales with the square of the bunch current squared multiplied by the repetition rate. To convert the neutrino factory into a muon collider, the basic repetition rate of 75 Hz is quite suitable, but one requires just one bunch in each cycle. If this can be done, and a six-dimensional emittance of $1.7 \times 10^{-10} (\pi m)^3$ can be achieved [16], a luminosity of $10^{31} \text{ cm}^{-2} \text{ s}^{-1}$ may be achieved, colliding beams with an energy spread of 0.01%.

In this report, we revisit first the physics prospects for $\mu^+\mu^-$ collider SM Higgs factories, examining in particular two effects that were overlooked in [7]. One is the WW^* decay mode, which is rather clean and has a branching ratio of at least 8% in the SM. The other is the effect of the beam energy spread, for which we consider values larger than the 0.003% considered previously. In this way, the range of SM Higgs masses for which useful measurements of the cross sections can be made extends up to about 160 GeV.

We recall that there is a richer Higgs sector in the MSSM, including three neutral Higgs bosons h , H and A , where the first two have scalar couplings in the CP-conserving limit, and the latter pseudoscalar couplings. As was also discussed in [7] there, are excellent prospects for a $\mu^+\mu^-$ collider tuned to the similar masses of the heavier neutral Higgs bosons H , A . If they weigh several hundred GeV or more, these might be difficult to observe and study at the LHC or a linear e^+e^- collider. A Higgs boson weighing as little as 115 GeV is not only *consistent* with supersymmetry, but even seems to *require* something very like it, if the effective Higgs potential is not to become unstable at a relatively low energy scale [17]. Thus, confirmation of the hint (1.2) would also be a strong encouragement to envisage a second $\mu^+\mu^-$ Higgs factory, even if the H and A have not been observed directly. In this context we study the influence of supersymmetric radiative corrections on the peak cross sections and branching ratios of h , H , A compared to a SM Higgs boson.

Both the first $\mu^+\mu^-h$ factory (FMC) and the second $\mu^+\mu^-(H, A)$ factory (SMC) will provide unique opportunities to study CP violation in the Higgs sector of the MSSM [7]. There have recently been improved studies of this possibility [18], in the light of which we revisit here the prospects for measuring various CP-violating observables at $\mu^+\mu^-$ colliders. Finally, we also discuss the prospects for measuring the H , A couplings to charginos at such a second $\mu^+\mu^-(H, A)$ factory.

2 CP-Conserving Studies

2.1 The $\mu^+\mu^- \rightarrow H \rightarrow X$ Cross Section

The effective cross section for Higgs production at $\sqrt{s} \sim m_H$ is obtained by convoluting the standard s -channel Breit-Wigner resonance with the beam energy distribution, which we model as a Gaussian distribution with width σ_E . At $\sqrt{s} = m_H$, initial-state radiation (ISR) effects can be approximated by a constant reduction factor η , where η is a function of the various parameters, $\alpha, m_H, m_\mu, \dots$, that we do not discuss here. In the limit $\Gamma \ll m_H$, quite a compact expression can be derived for the peak cross section:

$$\sigma_{\text{peak}} = \sigma(\sqrt{s} = m_H) = \frac{4\pi B(H \rightarrow \mu^+\mu^-) B(H \rightarrow X)}{m_H^2} \eta \pi^{1/2} A e^{A^2} (1 - \text{Erf}(A)), \quad (2.3)$$

where

$$A = \frac{1}{2\sqrt{2}} \frac{\Gamma}{\sigma_E} \quad \text{and} \quad \text{Erf}(x) = \frac{2}{\sqrt{\pi}} \int_0^x e^{-t^2} dt. \quad (2.4)$$

The peak cross section depends critically on the beam-energy spread σ_E compared to the resonance width Γ . There are two important limits:

$$\sigma_E \ll \Gamma \Rightarrow \sigma_{\text{peak}} = \frac{4\pi \eta B(H \rightarrow \mu^+\mu^-) B(H \rightarrow X)}{m_H^2}, \quad (2.5)$$

$$\sigma_E \gg \Gamma \Rightarrow \sigma_{\text{peak}} = \frac{\sqrt{2\pi^3} \eta \Gamma B(H \rightarrow \mu^+\mu^-) B(H \rightarrow X)}{m_H^2 \sigma_E}. \quad (2.6)$$

Figure 2(a) shows the \sqrt{s} dependence of $\sigma(\mu^+\mu^- \rightarrow H \rightarrow b\bar{b})$ for a SM Higgs boson H_{SM} weighing 115 GeV, compared with that the lightest MSSM Higgs boson, denoted here by H_{MSSM} , for various values of the beam-energy resolution $R \equiv \sqrt{2} \sigma_E / \sqrt{s}$. ISR is neglected. The peak cross section is plotted as a function of R in Fig. 2 (b). As can be seen, σ_{peak} reaches a plateau for $R \ll \Gamma_{bb}/m_H$, in accordance with (2.5), (2.6). Note also that the resonance is washed out in the limit $\Gamma/\sigma_E \rightarrow 0$.

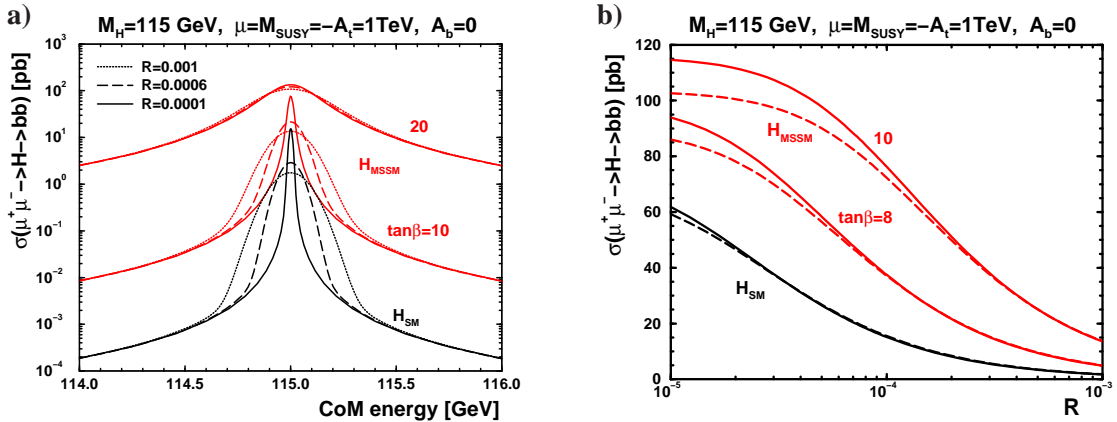


Fig. 2: (a) Cross sections for $\mu^+\mu^- \rightarrow H \rightarrow b\bar{b}$ as functions of \sqrt{s} for SM and MSSM Higgs bosons, and (b) R dependences of the peak cross sections, for $\overline{m}_b(\overline{m}_b) = 4.15$ GeV (solid lines) and $\overline{m}_b(\overline{m}_b) = 4.45$ GeV (dashed lines).

As has been discussed previously, not only is the beam energy spread at a $\mu^+\mu^-$ collider potentially very small, but also the energy can be calibrated very accurately using the decays of polarized muons in the circulating

beams. The very fine energy resolution and precision in \sqrt{s} expected at the $\mu^+\mu^-$ collider would allow the properties of the Higgs boson(s) to be determined with outstanding accuracy. One expects, for instance, to be able to measure the mass and width of a light ($m_H < 2 M_W$) Higgs boson to fractions of an MeV. If $\sigma_E \lesssim \Gamma$, the best procedure is to simply scan the resonance, as was studied in detail in [19, 6, 7, 8]. For a very narrow resonance, e.g., for a light SM Higgs boson, it may, however, be that $\sigma_E \lesssim \Gamma$ can only be achieved with substantial loss of luminosity. In this case it is of advantage to operate the collider at $\sqrt{s} = m_H$ and two different beam energy resolutions $\sigma_E^{\min} \ll \Gamma$ and $\sigma_E^{\max} \gg \Gamma$ [20]. One can then determine the width of the resonance from the ratio of the peak cross sections:

$$\sigma_{\text{peak}}(\sigma_E^{\min})/\sigma_{\text{peak}}(\sigma_E^{\max}) = [2\sqrt{2}\sigma_E^{\min}]/[\sqrt{\pi}\Gamma]. \quad (2.7)$$

The width of the SM Higgs boson is shown as a function of its mass in Fig. 3(a), as a line with triangles. Also shown, with solid circles, is the spread in the centre-of-mass energy for a collider with $R = 0.003\%$. The open squares correspond to the spread in the centre-of-mass energy which is obtained if R is varied so that the beam energy spread is always 40% of the Higgs width. It is assumed here that any value of R can be obtained, and that the luminosity scales as $R^{2/3}$. This procedure approximately optimises the Higgs production rate, and hence the statistical error on the Higgs cross-section. Tighter beam energy spreads have lower luminosities, while increasing the spread reduces the Higgs cross-section. Figure 3(b) shows how the reduction factor given in (2.3) reduces the peak cross section in the two cases.

The decay mode $H \rightarrow b\bar{b}$ was investigated in [7], and those results are updated in Fig. 3(c), taking account of the loss in peak cross section. The suppression is less important as the mass, and hence the width, rises. This means that the performance for $m_H = 140$ GeV is almost the same as for $m_H = 115$ GeV. We also display results for the WW^* decay mode, which is rather clean and has at least an 8% branching ratio in the SM. The accuracy of the width measurement obtainable at a $\mu^+\mu^-$ collider in this channel is estimated by assuming that the efficiency and background achieved by the DELPHI collaboration in measuring WW production at 161 GeV [21] can be duplicated. This includes the conservative assumption that the spin information is not used to reduce the non-resonant WW background. We note that for $M_H = 115$ GeV a 6% error on the $b\bar{b}$ cross-section and 32% on the WW^* are expected per 300 pb^{-1} , or three years of running.

The decay mode $H \rightarrow \tau^+\tau^-$ is also an important channel, which provides power to distinguish between different Higgs models [22]. The importance of this decay mode is discussed in more detail in [23] and in Sect. 2.3, but we recall here that a measurement of the branching ratio with a 16% statistical error could be made at a $\mu^+\mu^-$ collider using an integrated luminosity of 100 pb^{-1} .

We conclude that if one varies R at centre-of-mass energies above ~ 145 GeV, useful cross section measurements are possible up to about 160 GeV. Beyond this point, the Higgs resonance is simply too wide for a peak cross-section measurement to be feasible. However, we can confidently expect at least one Higgs boson in the mass range accessible to a $\mu^+\mu^-$ collider.

The accuracies for the branching ratio measurements have to be compared with the corresponding numbers at an e^+e^- linear collider [3, 4, 5], where $\Delta BR/BR$ of about 2.5%, 5%, 4% are achievable for the $b\bar{b}$, $\tau^+\tau^-$, WW^* modes respectively (for $m_H = 120$ GeV, $\sqrt{s} = 350$ GeV, and $\int \mathcal{L} = 500 \text{ fb}^{-1}$). We emphasize that the FMC accuracies quoted earlier for these modes are very dependent on the luminosity obtainable, and that these LC numbers include detailed detector simulations that are not yet available for the FMC. In addition, by combining LC and FMC data the branching ratio of $H \rightarrow \mu^+\mu^-$ can be measured to 4% accuracy [8].

It was observed in [7] that, for certain values of R , $\sigma_{\text{peak}}(\mu^+\mu^- \rightarrow H \rightarrow b\bar{b})$ becomes practically independent of m_b . More generally speaking, R can be chosen such that the peak cross section for a given final state X is

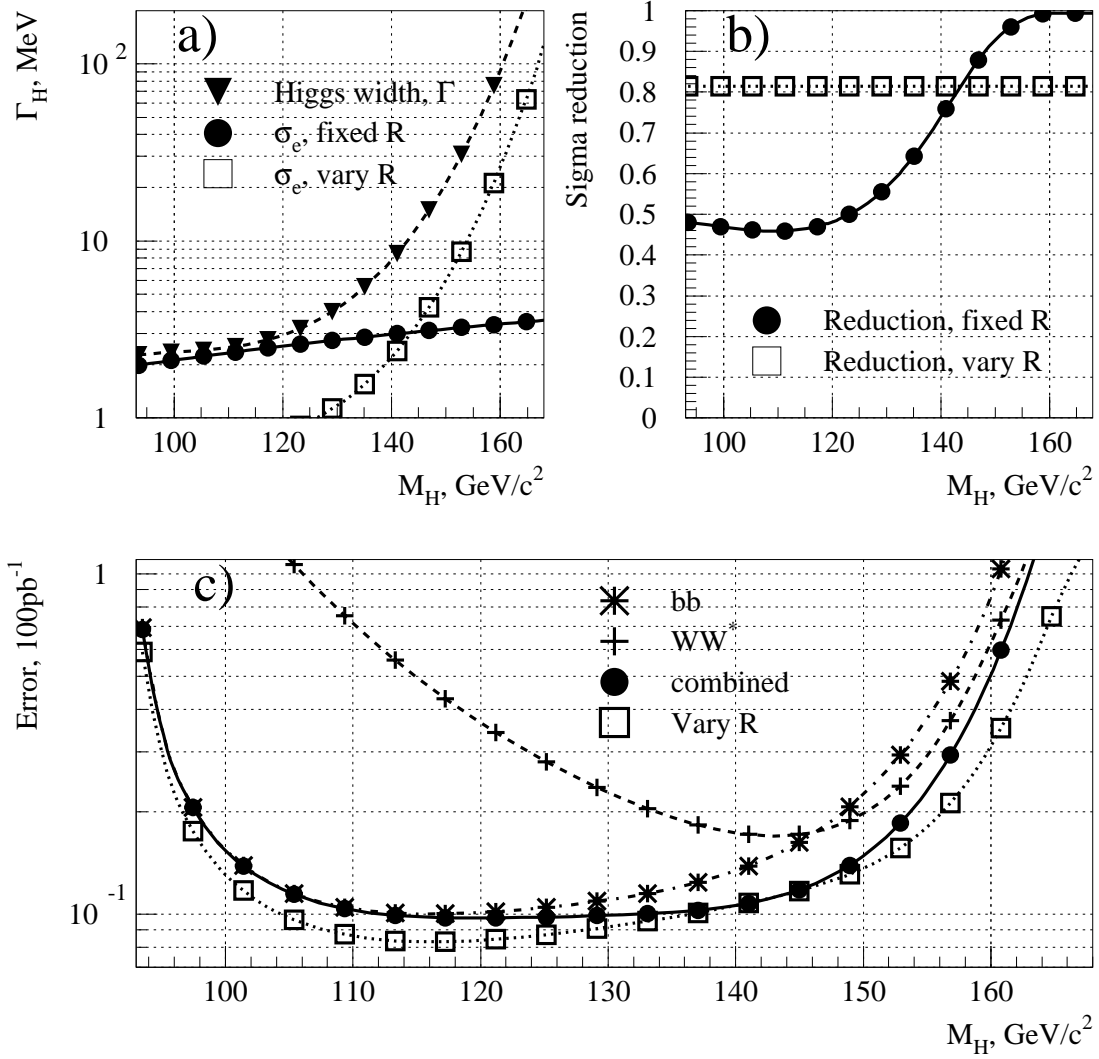


Fig. 3: Plot (a) shows the width of the SM Higgs boson as a function of its mass (triangles), the centre-of-mass energy spread for $R = 0.003\%$ (filled circles) and the optimal varying energy spread (open squares). Plot (b) shows the cross-section suppression factor due to the width of the beams if $R = 0.003\%$ (filled circles), and for the optimal varying R (open squares). Plot (c) shows the fractional error with which the Higgs cross section can be measured in the $b\bar{b}$ (stars) and WW^* decay modes (crosses) using 100 pb^{-1} of data obtained with $R = 0.003\%$. The solid circles shows the accuracy with which the peak cross section can be extracted if the SM branching ratios are assumed, and the open squares show the error obtained in the same running period by optimizing R .

insensitive to Γ_X , i.e. $d\sigma_{\text{peak}}/d\Gamma_X = 0$, or equivalently

$$\frac{\Gamma}{\Gamma_X} - 1 = \frac{2A}{\sqrt{\pi}} \frac{e^{-A^2}}{1 - \text{Erf}(A)} - 2A^2. \quad (2.8)$$

In practice, this is only relevant if (i) $H \rightarrow X$ is the dominant decay channel, $B(H \rightarrow X) > 0.5$, and (ii) $\sigma_E \lesssim \Gamma_X$. For both H_{SM} and H_{MSSM} these conditions can be simultaneously fulfilled only for $X = b\bar{b}$. Figure 4(a) shows contours of $d\sigma_{\text{peak}}/d\Gamma_{bb} = 0$ in the m_H - R plane for various values of $\tan\beta$. Assuming a conservative error

in the $\overline{\text{MS}}$ bottom mass determination, namely $\overline{m}_b(\overline{m}_b) = 4.30 \pm 0.15$ GeV, would imply a 15% indeterminacy in the $\Gamma(H \rightarrow b\bar{b})$ partial width. If the accelerator parameters are tuned in such a way that (2.8) is fulfilled, the impact of this uncertainty on the theoretical prediction for the value of the $\mu^+\mu^- \rightarrow H \rightarrow b\bar{b}$ peak cross section is minimized. This is illustrated in Fig. 4 b for a MSSM Higgs boson with a mass of 110 GeV, for $\tan\beta = 8$, and $R = 8.5 \cdot 10^{-3}$.

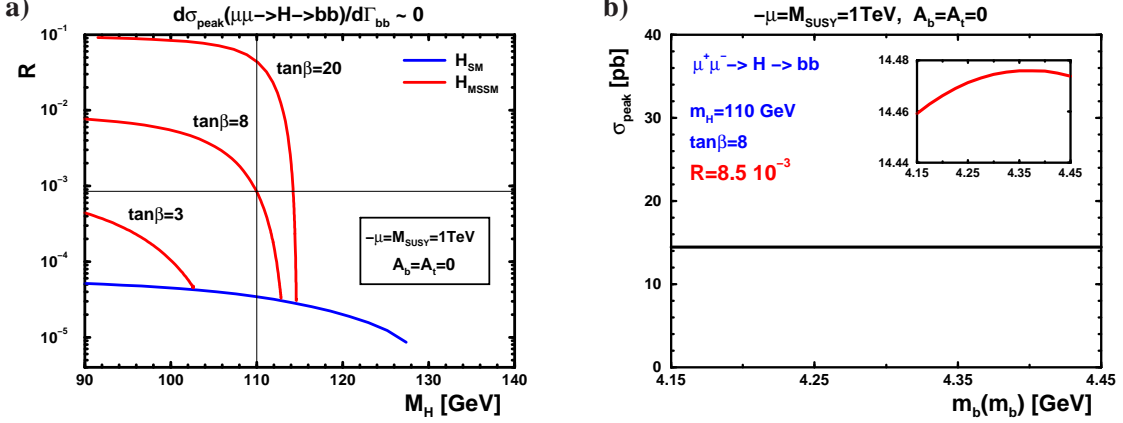


Fig. 4: (a) Points in the m_H - R plane where the $\mu^+\mu^- \rightarrow H \rightarrow b\bar{b}$ cross section has a local maximum in the variable m_b . Curves are shown for the lightest neutral MSSM Higgs (assuming CP conservation) and for the SM Higgs. In the former case, the relevant MSSM parameters are shown in the plot. The crossing vertical and horizontal lines pick up one such point for the MSSM Higgs. In (b), the m_b dependence of the peak cross section is shown for that point.

In this way, the $\mu^+\mu^- \rightarrow H \rightarrow b\bar{b}$ peak cross section may be used as a precision measurement that may be interpreted, for example to constrain MSSM parameters as we discuss later, without any ambiguity related to m_b .

2.2 Radiative Corrections to $\mu^+\mu^- \rightarrow h$

Given the excellent experimental accuracy expected for a $\mu^+\mu^-$ collider, quantum corrections to the Higgs production and decay processes have to be taken into account. For definiteness, we concentrate here on the quantum corrections in the MSSM, assuming CP conservation, and leaving the extension to include explicit CP violation induced by loop effects to section 3 of this report. We discuss how quantum corrections affect the Higgs production cross sections and how they alter the Higgs branching ratios. Since these corrections depend on the underlying supersymmetry parameters, precise measurements of the Higgs boson masses, widths, branching ratios, *etc.* may be used to pin down the parameter space of the MSSM. They may also be used for important consistency checks of the model.

We focus on the three neutral Higgs bosons expected in the MSSM in the CP-conserving limit, namely the two scalars h and H , and the pseudoscalar A . Table 1 shows their tree-level couplings to up- and down-type quarks/leptons and to the W^\pm and Z bosons, relative to those of a SM Higgs boson. Here $\tan\beta \equiv v_2/v_1$ and α diagonalizes the CP-even Higgs sector, $h = -\sin\alpha H_1^0 + \cos\alpha H_2^0$, $H = \cos\alpha H_1^0 + \sin\alpha H_2^0$. In the limit $m_A \rightarrow \infty$, H and A (and H^\pm) decouple from low-energy physics, whilst h becomes SM-like. At tree level, one has $m_h \rightarrow m_Z |\cos 2\beta|$ and $\alpha \rightarrow \beta - \pi/2$ in this case.

The CP-even Higgs mass matrix \mathcal{M}^2 is, however, subject to large radiative corrections, the leading effects being $\propto h_t^4$ [14], with h_t the top Yukawa coupling. A one-loop renormalization-group- (RG-)improved effective

	t	$b, \tau(\mu)$	W, Z
h^0	$\cos \alpha / \sin \beta$	$-\sin \alpha / \cos \beta$	$\sin(\beta - \alpha)$
H^0	$\sin \alpha / \sin \beta$	$\cos \alpha / \cos \beta$	$\cos(\beta - \alpha)$
A^0	$-i\gamma_5 \cot \beta$	$-i\gamma_5 \tan \beta$	0

Table 1: Tree-level couplings of the MSSM Higgs bosons h , H , and A relative to those of a SM Higgs boson.

potential calculation gives [25]

$$\begin{aligned} \mathcal{M}_{12}^2 \sim & - \left[m_A^2 + m_Z^2 - \frac{h_t^4 v^2}{8\pi^2 M_{\text{SUSY}}^2} \mu^2 \left(3 - \frac{A_t^2}{M_{\text{SUSY}}^2} \right) \right] \sin \beta \cos \beta \\ & + \xi \left[\frac{h_t^4 v^2}{16\pi^2} \sin^2 \beta \frac{\mu A_t}{M_{\text{SUSY}}^2} \left(\frac{A_t^2}{M_{\text{SUSY}}^2} - 6 \right) + 3 \frac{h_t^2 m_Z^2}{32\pi^2} \frac{\mu A_t}{M_{\text{SUSY}}^2} \right] \end{aligned} \quad (2.9)$$

where ξ accounts for the leading-logarithmic two-loop effects, M_{SUSY} is an overall supersymmetry scale, and A_t is the trilinear soft SUSY-breaking parameter in the stop mass matrix. Diagonalizing the loop-corrected \mathcal{M}^2 gives the higher-order values of m_h , m_H , and the effective mixing angle α_{eff} , with

$$\sin 2\alpha_{\text{eff}} = \frac{2\mathcal{M}_{12}^2}{\sqrt{(\text{Tr} \mathcal{M}^2)^2 - 4 \det \mathcal{M}^2}}. \quad (2.10)$$

As has been shown analytically in [24], if supersymmetric vertex corrections are neglected, the improved tree-level couplings are obtained by replacing $\alpha \rightarrow \alpha_{\text{eff}}$ in Table 1. Note, however, that the vertex corrections may well be important, as is discussed for the $hb\bar{b}$ and $h\tau^+\tau^-$ vertices in Sect. 2.3.

While in a large fraction of the MSSM parameter space the couplings of h to $b\bar{b}$, $\mu^+\mu^-$, $\tau^+\tau^-$ are enhanced compared to those of a SM Higgs boson, it is, according to (2.9), also possible to have $\mathcal{M}_{12}^2 \rightarrow 0$, which corresponds to $\sin \alpha_{\text{eff}} \rightarrow 0$ or $\cos \alpha_{\text{eff}} \rightarrow 0$. Thus g_{hbb} , $g_{h\tau\tau}$ or $g_{h\mu\mu}$ can be strongly reduced in the MSSM [25, 26]. This could lead to a highly suppressed production cross section for the lightest CP-even Higgs boson, even if it is in the kinematically accessible region.

We display in Fig. 5 the regions of parameter space where $\sigma_{\text{MSSM}}(\mu^+\mu^- \rightarrow h)/\sigma_{\text{SM}}(\mu^+\mu^- \rightarrow h) < 30\%$ (for details, see [27]). Results obtained with the `FeynHiggs` code [28] are displayed in the m_A - $\tan\beta$ plane for $M_{\text{SUSY}} = 300, 1000$ GeV. The off-diagonal entry in the \tilde{t} mass matrix is taken as $X_t \equiv A_t - \mu/\tan\beta = \pm M_{\text{SUSY}}, 2M_{\text{SUSY}}$. Moreover, we choose $\mu = 2M_{\text{SUSY}}$ and $A_b = A_t$. The other MSSM parameters are $M_2 = 400$ GeV and $m_{\tilde{g}} = M_{\text{SUSY}}$, and we take $m_t = 175$ GeV and $\overline{m}_b = \overline{m}_b(m_t) = 2.97$ GeV.

The top plots in Fig. 5 show the case with a relatively small supersymmetry mass scale, $M_{\text{SUSY}} = 300$ GeV, for the two combinations $X_t = \mu = 600$ GeV and $X_t = -300$ GeV, $\mu = 600$ GeV. In general, the regions with $\sigma(\mu^+\mu^- \rightarrow h) < 30\%$ are obtained for large $\tan\beta \gtrsim 15$ and relatively small m_A : $100 \text{ GeV} \lesssim m_A \lesssim 300 \text{ GeV}$. This follows from (2.9) in the limit $\mathcal{M}_{12}^2 \rightarrow 0$, since m_A has to be relatively small in order for the higher-order corrections to be of a size similar to $(m_A^2 + m_Z^2) \sin \beta \cos \beta$. Due to the functional dependence of \mathcal{M}_{12}^2 on μ and $X_t \approx A_t$ for $\tan\beta \gtrsim 10$ as seen in (2.9), the regions hardly change their shape if both X_t and μ change their sign. However, their shape and location change drastically if only one sign flips. In the bottom plot in Fig. 5, we show the corresponding regions for a large supersymmetry mass scale, $M_{\text{SUSY}} = 1000$ GeV, and $X_t = \mu = 2000$ GeV. As in the low M_{SUSY} case, we find a non-negligible part of parameter space with a highly suppressed $\sigma(\mu^+\mu^- \rightarrow h)$ ¹.

¹The regions in Fig. 5 with suppressed production cross section are not significantly affected by the exclusion bounds obtained from the Higgs search at LEP [11, 29].

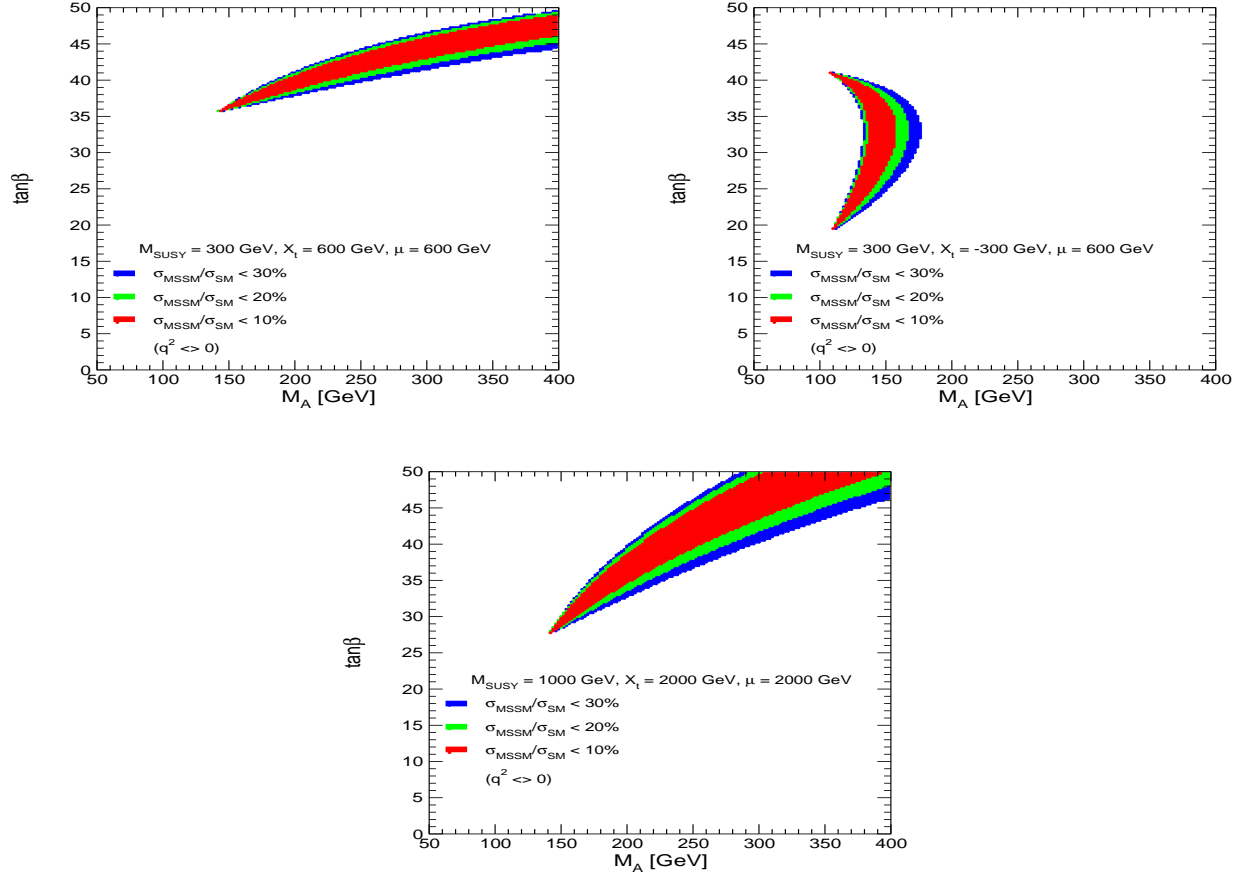


Fig. 5: Regions in the m_A - $\tan\beta$ plane where $\sigma_{\text{MSSM}}(\mu^+\mu^- \rightarrow h)/\sigma_{\text{SM}}(\mu^+\mu^- \rightarrow h) < 30\%$ for a common supersymmetric mass scale $M_{\text{SUSY}} = 300$ GeV (top) and $M_{\text{SUSY}} = 1000$ GeV (bottom).

A more extensive discussion can be found in Ref. [27].

The parameter regions where $\sigma(\mu^+\mu^- \rightarrow h)$ goes to zero are clearly somewhat unusual, and this possibility is not realized in the constrained MSSM (CMSSM), in which the soft supersymmetry-breaking scalar masses m_0 and gaugino masses $m_{1/2}$ are required to be universal at an input GUT scale [30]. This is exemplified in Fig. 6, where we show $[\sigma(\mu^+\mu^- \rightarrow h) \times \text{B}(h \rightarrow b\bar{b})]_{\text{CMSSM}}$ in terms of standard deviations from the SM value in the $m_{1/2} - m_0$ plane for $\mu > 0$ and two combinations of $\tan\beta$ and A_0 , together with the constraints from $\text{B}(b \rightarrow s\gamma)$ [31, 32], $g_\mu - 2$ [33] and the requirement that the LSP is uncolored and uncharged [34]. The mass of the lightest MSSM Higgs boson is also indicated [28]. We have assumed an accuracy of 3% [7] in the determination of $\sigma(\mu^+\mu^- \rightarrow h) \times \text{B}(h \rightarrow b\bar{b})$. No suppression of Higgs production can be observed for the CMSSM parameter space. On the contrary, the production and decay is always enhanced compared to the corresponding SM value, over the entire CMSSM parameter space [30]. However, the existence in principle of the regions in the unconstrained MSSM with suppressed Higgs production cross section does point up the interest of measuring this observable.

We note also that, even when $\sigma(\mu^+\mu^- \rightarrow h)$ does vanish, the production cross sections of H and A are unsuppressed and even enhanced by $\tan\beta$. Moreover, H and A would mainly decay into $b\bar{b}$ or $\tau^+\tau^-$. We find that in this case the usual mass hierarchy between H and A is inverted: The CP-odd Higgs-boson mass m_A

turns out to be larger than m_H by up to 25 GeV. For a considerable fraction of the parameter regions with suppressed $\sigma(\mu^+\mu^- \rightarrow h)$, the mass splitting $m_A - m_H$ is larger than the sum of the total widths of A and H (this holds in particular for not too large values of $\tan\beta$). Thus, in these regions A and H should not only be produced with sufficiently high rates but should also be resolvable as separate resonances. Even in the regions where $\sigma(\mu^+\mu^- \rightarrow h)$ is suppressed, the $\mu^+\mu^-$ collider would therefore possess a promising potential for probing the neutral MSSM Higgs sector via resonant production of H and A . This is illustrated in Fig. 7, where the peak cross sections of $\mu^+\mu^- \rightarrow \{h, H \text{ or } A\} \rightarrow b\bar{b}$ are shown as a function of $\tan\beta$ for $m_A = 140$ GeV and $M_{\text{SUSY}} = \mu = -A_t = 1$ TeV. Note that, for a large range of values of $\tan\beta$, the $\mu^+\mu^- \rightarrow h \rightarrow b\bar{b}$ cross section is much larger than that of a SM Higgs boson of the same mass. For $\tan\beta \sim 60$, however, $\sin\alpha_{\text{eff}} \sim 0$ and $\sigma(\mu^+\mu^- \rightarrow h)$ vanishes. On the other hand, $\sigma_{\text{peak}}(\mu^+\mu^- \rightarrow H, A \rightarrow b\bar{b})$ increases almost linearly for $\tan\beta \gtrsim 10$.

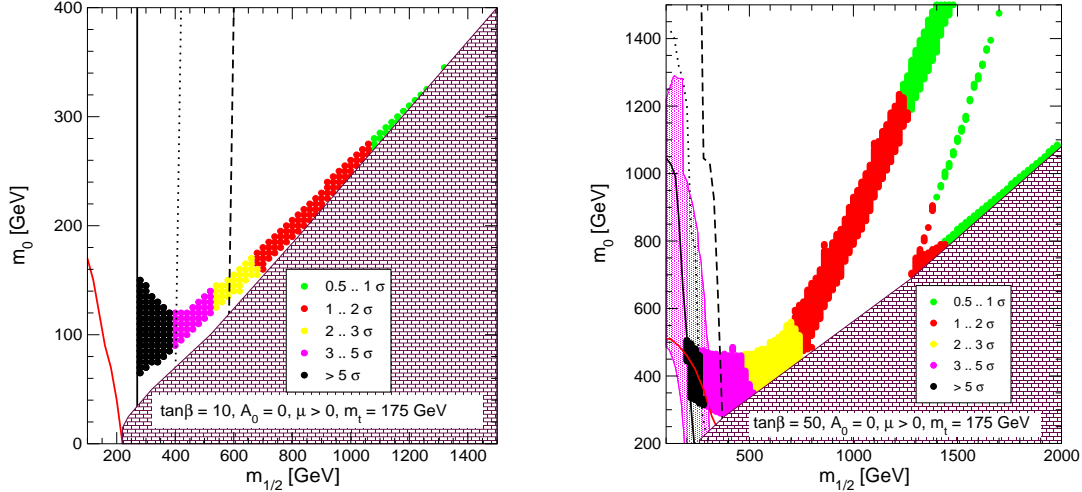


Fig. 6: $[\sigma(\mu^+\mu^- \rightarrow h) \times \text{B}(h \rightarrow b\bar{b})]_{\text{CMSSM}}$ compared to the SM value in the $m_{1/2} - m_0$ plane for $\mu > 0$ and $\tan\beta = 10$, $A_0 = 0$ (left plot) and $\tan\beta = 50$, $A_0 = -2m_{1/2}$ (right plot) [30], assuming an experimental accuracy of 3%. The bricked region is forbidden because the LSP is the lightest $\tilde{\tau}$. The regions above and to the right of the (red) diagonal solid lines yield values of $g_\mu - 2$ within 2σ of the present central value. The light shaded (pink) region is excluded by $\text{B}(b \rightarrow s\gamma)$ measurements. The solid leftmost (dotted middle, dashed rightmost) near-vertical line corresponds to $m_h = 113$ (115, 117) GeV [28].

2.3 Corrections to the hbb and $h\tau^+\tau^-$ Vertices

An interesting topic that could be investigated at a $\mu^+\mu^-$ collider is the effect of supersymmetric threshold corrections on the Yukawa interactions. For large $\tan\beta$ and μ one expects relative deviations of order unity of the couplings from their tree-level values, due to gluino (SUSY-QCD) and, to a lesser extent, higgsino (SUSY-EW) radiative effects.² Such deviations would be strongly correlated, as discussed below, allowing for non-trivial self-consistency checks of the model. Moreover, these corrections should of course be taken into account when determining the underlying SUSY parameters from the Higgs bosons production cross sections and branching ratios.

It can be proven that, in mass-independent renormalization schemes like $\overline{\text{MS}}$, all-order SUSY corrections of

²Large- $\tan\beta$ scenarios, like those derived from some supersymmetric SO(10) models [35, 36], have become more appealing since LEP searches for a light neutral Higgs boson started excluding the low- $\tan\beta$ region of the MSSM parameter space [29].

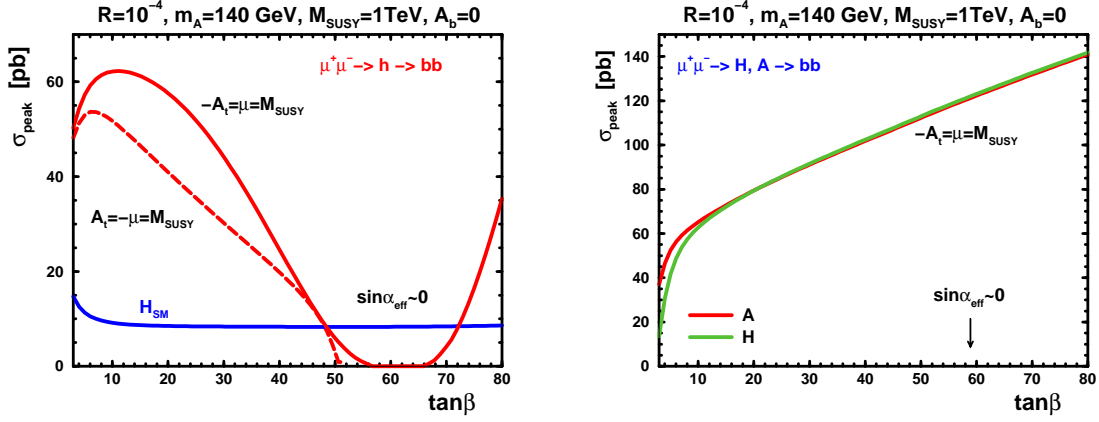


Fig. 7: The $\tan \beta$ dependence of the $\mu^+ \mu^- \rightarrow (h, H, A) \rightarrow b \bar{b}$ peak cross sections. The H_{SM} curve has a small dependence on $\tan \beta$ on the left, reflecting the fact that we set the SM Higgs mass equal to M_h .

the form $\alpha_S^n \tan^n \beta$ can be resummed in the following definition for h_b [37]:

$$h_b v_1 = \frac{m_b}{1 + \Delta h_b^1/h_b + \Delta h_b^2/h_b \tan \beta} \sim \frac{m_b}{1 + \Delta m_b}, \quad (2.11)$$

with the quantity Δm_b being dominated by SUSY-QCD virtual effects:³

$$\Delta m_b \sim \Delta m_b^{\text{SQCD}} = \frac{2\alpha_S}{3\pi} \mu m_{\tilde{g}} \tan \beta I(m_{\tilde{b}_1}, m_{\tilde{b}_2}, m_{\tilde{g}}), \quad (2.12)$$

where I is the limit of the Passarino-Veltman function C_0 for vanishing external momenta. It can be shown that Δm_b does not vanish in the limit $M_{\text{SUSY}} \rightarrow \infty$. In fact, it approaches $\alpha_S/(3\pi) \tan \beta$ asymptotically. This should not be understood as a non-decoupling effect, as its physical consequences in low-energy observables do vanish in the limit $m_A \rightarrow \infty$, when the SM is recovered as an effective theory, as discussed below. There is, however, an important phenomenological consequence of the non-vanishing behaviour of (2.12): even for a very heavy supersymmetric spectrum (but not too large m_A), one expects large deviations from the normal ratio

$$g_{hbb}/g_{h\tau\tau} = m_b/m_\tau, \quad (2.13)$$

which holds not only in the SM, but also in two-Higgs-doublet models (2HDMs) of types I and II [38]. This translates for instance, into the corresponding ratio of branching fractions, as can be seen in Fig. 8. Since this ratio may be measurable with a precision better than 16%, as mentioned previously, multi-standard-deviation discrimination between the MSSM and the SM is possible for small m_A .

Using (2.11), and after adding the process-dependent SUSY vertex corrections, the renormalized amplitudes for $h \rightarrow b \bar{b}$, $H \rightarrow b \bar{b}$ and $A \rightarrow b \gamma_5 \bar{b}$ read [25]:

$$\mathcal{A}(\bar{b} b h) \sim \frac{m_b}{v} \frac{\sin \alpha_{\text{eff}}}{\cos \beta} \frac{1}{1 + \Delta m_b} \left(1 - \frac{\Delta m_b}{\tan \alpha_{\text{eff}} \tan \beta} \right), \quad (2.14)$$

$$\mathcal{A}(\bar{b} b H) \sim -\frac{m_b}{v} \frac{\cos \alpha_{\text{eff}}}{\cos \beta} \frac{1}{1 + \Delta m_b} \left(1 + \Delta m_b \frac{\tan \alpha_{\text{eff}}}{\tan \beta} \right), \quad (2.15)$$

$$\mathcal{A}(i \bar{b} \gamma_5 b A) \sim \frac{m_b}{v} \tan \beta \frac{1}{1 + \Delta m_b}. \quad (2.16)$$

³A similar formula can be written for the τ Yukawa coupling, although the SUSY-EW contributions in Δm_τ are (generally) smaller.

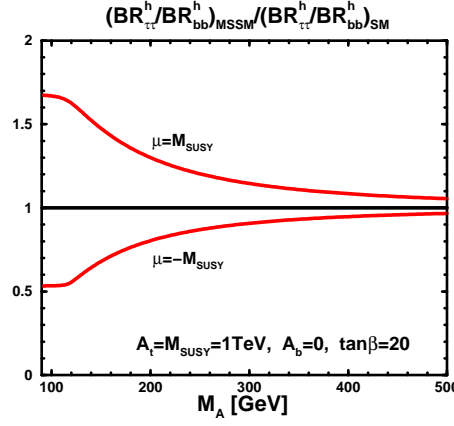


Fig. 8: Ratio of the $h \rightarrow \tau^+\tau^-$ and $h \rightarrow b\bar{b}$ branching ratios in the MSSM relative to those in the SM.

As can be checked in (2.14) one recovers the SM coupling for $h b \bar{b}$ (and $G^0 b \bar{b}$) as $m_A/M_W \rightarrow \infty$, because $\tan \alpha_{\text{eff}} \rightarrow -1/\tan \beta$. We see in (2.14) how a radiative zero of the $\mu^+\mu^- \rightarrow h \rightarrow b\bar{b}$ cross section could occur if

$$\tan \alpha_{\text{eff}} = \frac{\Delta m_b}{\tan \beta} \implies g_{hbb} \sim 0. \quad (2.17)$$

At the same time, $g_{h\mu\mu}$ and $g_{h\tau\tau}$ are not zero but

$$g_{h\tau\tau(\mu\mu)} = \frac{m_{\tau(\mu)}}{v} \frac{\Delta m_b - \Delta m_{\tau(\mu)}}{1 + \Delta m_{\tau(\mu)}}. \quad (2.18)$$

For $\Delta m_b \sim \mathcal{O}(1)$, this is of the same order as the corresponding coupling in the SM. Hence $\sigma(\mu^+\mu^- \rightarrow h)$ is not suppressed, but h does not decay into $b\bar{b}$. Instead, it mainly decays into $\tau^+\tau^-$ or WW^* . The total decay width, however, becomes very small, of the order of a few MeV, leading to an extremely narrow resonance even for large $\tan \beta$. An example is shown in Fig. 9, where we plot $\sigma_{\text{peak}}(\mu^+\mu^- \rightarrow h)$ as a function of $\delta\sqrt{s} \equiv \sqrt{s} - m_h$ for various $\tan \beta$ values. Notice that, for small Γ_h values, the actual width of the resonances is approximately given by $R\sqrt{s} \sim \sigma_E$ (see (2.6)).

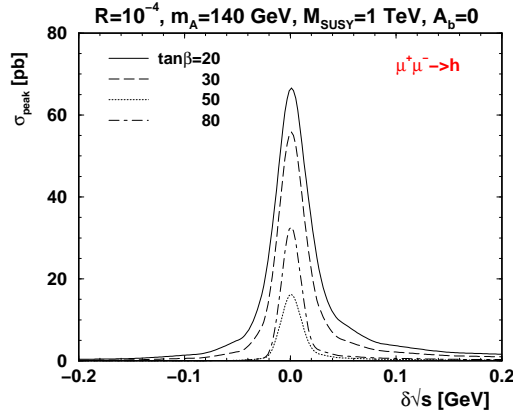


Fig. 9: Resonant $\mu^+\mu^- \rightarrow h$ cross sections, for $\tan \beta = 20, 30, 50, 80$, as a function of the distance to the peak of the resonance, $\delta\sqrt{s}$. The remaining MSSM parameters are chosen as in Fig. 7.

Last but not least, it should be mentioned that the treatment of the vertex corrections in terms of $\Delta m_{b(\tau)}$ is a very good approximation for large $\tan \beta$ and $M_{\text{SUSY}} \gg m_A$. For $M_{\text{SUSY}} \sim m_A$, however, this should be

complemented with the remaining neglected terms in a full one-loop computation [24, 39]. Here the problem of a consistent treatment of the stop and sbottom system arises. For a prescription which includes a consistent renormalization of the \tilde{t} and \tilde{b} sectors and which is, moreover, valid for all allowed $\tan\beta$ values, see [40].

3 CP Violation at $\mu^+\mu^-$ Colliders

3.1 Introduction

In this Section, we discuss ways in which models of CP violation may be probed at both the FMC and the SMC. We recall that, although the effective Higgs potential of the Standard Model (SM) conserves CP, at least up to the two-loop level, this symmetry is generically violated in models which extend the Higgs sector even minimally, such as the two-Higgs-doublet model [41]. Very interestingly, even though CP symmetry can be imposed on the complete Lagrangian of a three-Higgs-doublet model, it can still be broken spontaneously by the Higgs ground state [42]. In supersymmetric theories, CP violation may be generated either spontaneously [43, 44] or explicitly [45, 18] via loop effects. In particular, the MSSM with explicit radiative CP breaking in the Higgs sector constitutes a prototype scenario for studying CP violation at a $\mu^+\mu^-$ machine. As we argue below, the option of muon polarization at a $\mu^+\mu^-$ collider would be a particularly valuable tool for determining the CP properties of Higgs bosons.

In this connection, we first review briefly the basic mechanism for obtaining resonantly-enhanced CP asymmetries in Higgs-mediated processes at the FMC. Then we discuss the CP-violating effects due to vertex corrections in the MSSM. Next we define optimal CP-violating observables based on muon polarization and give estimates of the expected CP violation in the MSSM and other extended scenarios. We also summarize the requirements for reducing the CP-conserving background. Finally, we give an example of the possible impact of CP violation on the mass difference between the second and third neutral Higgs bosons in the MSSM with CP violation [18].

3.2 Resonant CP Violation due to Higgs-Mass Mixing

The general formalism for mass mixing in extended Higgs sectors with explicit CP violation induced by loop effects is well developed [46, 45]. It is instructive for our purposes here to recall the conditions necessary for CP asymmetries to exhibit resonant enhancement. For this purpose, we consider a generic process $ab \rightarrow 12$, as shown in Fig. 10. Such a reaction may proceed via both CP-even and CP-odd Higgs bosons, H and A , as intermediate states. The corresponding transition amplitude may be written as

$$\mathcal{T} = \mathcal{T}^{res} + \mathcal{T}^{box} = V_i^P \left(\frac{1}{s - \mathcal{H}(s)} \right)_{ij} V_j^D + \mathcal{T}^{box}, \quad (3.19)$$

where

$$s - \mathcal{H}(s) = \hat{\Delta}^{-1}(s) = s\mathbf{1} - \begin{bmatrix} M_A^2 - \hat{\Pi}^{AA}(s) & -\hat{\Pi}^{AH}(s) \\ -\hat{\Pi}^{HA}(s) & M_H^2 - \hat{\Pi}^{HH}(s) \end{bmatrix} \quad (3.20)$$

is the inverse-propagator matrix, which describes the dynamics of the $H - A$ mass mixing.⁴ The propagator matrix $\hat{\Delta}(s)$ actually arises from summing a geometric series of HH , AA , HA and AH self-energies. In (3.20), the hat symbol $\hat{}$ denotes the fact that the resummed self-energies should be renormalized within a gauge-invariant resummation approach that respects unitarity [46], e.g., the one implemented by the Pinch Technique (PT) [48].

⁴For a full discussion, including three-state $h - H - A$ mixing, see [47].

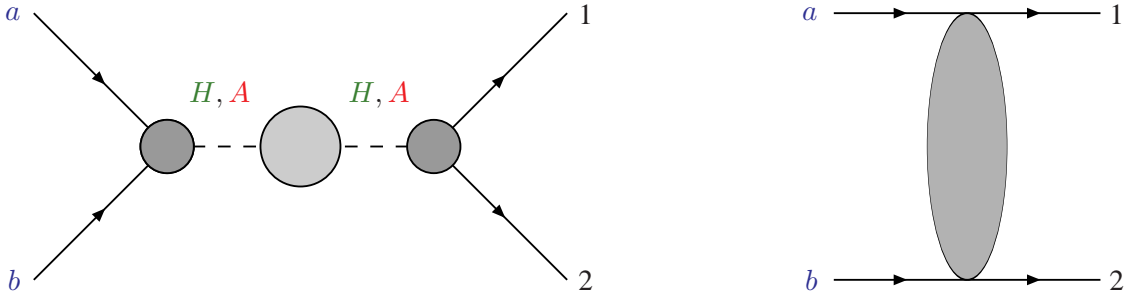


Fig. 10: Resonant and non-resonant Higgs contributions to a generic process $ab \rightarrow 12$.

Assuming that the non-resonant term \mathcal{T}^{box} in (3.19) is negligible, we may identify two sources of CP violation: (i) the non-vanishing scalar-pseudoscalar mixing term $\hat{\Pi}^{AH}(s)$ in the effective Higgs-boson mass matrix, and (ii) CP violation in the production and decay vertices V_i^P and V_i^D . By analogy with the neutral kaon system, we term these ε - and ε' -type effects, respectively. We first discuss the ε -type effects, which will be resonantly enhanced if [46]

$$|M_H^2 - M_A^2 - \hat{\Pi}^{HH}(s) + \hat{\Pi}^{AA}(s)| \lesssim 2|\hat{\Pi}^{HA}(s)|. \quad (3.21)$$

The condition (3.21) is naturally fulfilled in models where the CP invariance of the Higgs potential is minimally lifted by radiative effects, such as the MSSM [45, 18] and heavy Majorana-neutrino models inspired by E_6 theories [46].

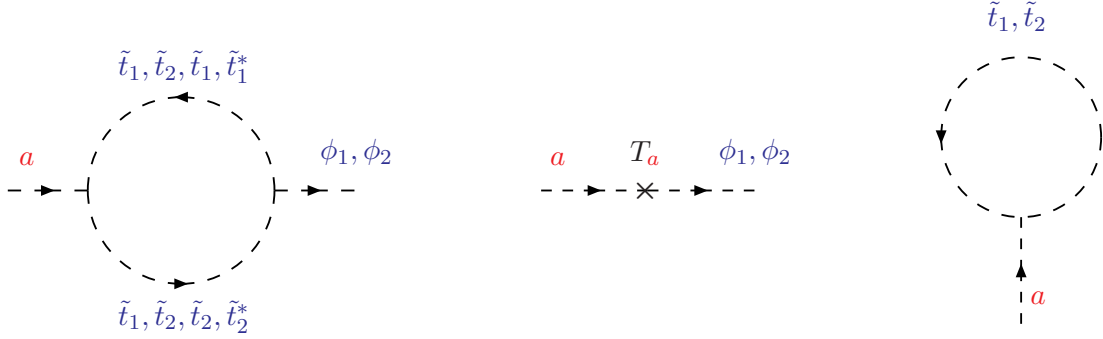


Fig. 11: One-loop contributions to scalar-pseudoscalar mixing in the MSSM.

In the constrained MSSM with universal soft supersymmetry-breaking masses m_0 for sfermions and $m_{1/2}$ for gauginos, as well as trilinear supersymmetry-breaking parameters A_i , there are two independent CP-violating phases. Without loss of generality, these may be taken as the phase of the gluino mass $m_{\tilde{g}}$ and A_t . As illustrated in Fig. 11, CP-violating scalar-pseudoscalar transitions $\mathcal{M}_{SP}^2 \sim \hat{\Pi}^{HA}(0)$ in the MSSM are predominantly induced by stop squarks. The qualitative behaviours of important CP-violating terms are given by

$$\mathcal{M}_{SP}^2 \sim \frac{m_t^4}{v^2} \frac{\text{Im}(\mu A_t)}{32\pi^2 M_{\text{SUSY}}^2} \left(1, \frac{|A_t|^2}{M_{\text{SUSY}}^2}, \frac{|\mu|^2}{\tan \beta M_{\text{SUSY}}^2}, \frac{2\text{Re}(\mu A_t)}{M_{\text{SUSY}}^2} \right), \quad (3.22)$$

where μ is the supersymmetric parameter characterizing the mixing of the two Higgs superfields, and M_{SUSY}^2 specifies the common soft supersymmetry-breaking scale defined by the arithmetic average of the squared stop masses. We see from (3.22) that \mathcal{M}_{SP}^2 could in principle be as large as M_Z^2 [45].

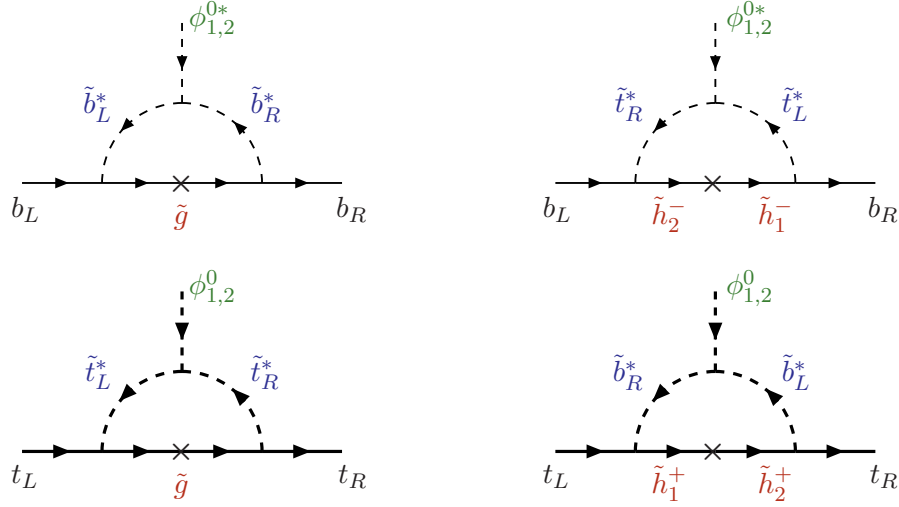


Fig. 12: CP-violating vertex effects on the bottom and top Yukawa couplings.

This is possible if the phase of A_t is large, which cannot be excluded *a priori*. There are important constraints on the CP-violating phases in the MSSM coming, in particular, from constraints on the electric dipole moments of the electron, neutron and ^{199}Hg [49]. However, cancellations are possible between different supersymmetric diagrams, and between different CP-violating operators [50, 51]. Moreover, the constraints apply directly only to the first and possibly second generation of matter fermions, and so may be more relaxed for the third-generation coupling A_t [52], if one relaxes the assumption of universality between the different generations.

Analogously, in heavy Majorana-neutrino models, scalar-pseudoscalar mixings are induced after integrating out the heavy Majorana neutrinos, and may also be non-negligible. However, we do not discuss such models in any further detail here.

3.3 CP-Violating Vertex Effects

In addition to the CP-violating self-energy effects, CP-violating vertex effects involving gluinos, higgsinos and squarks of the third generation [18] may drastically modify the top- and bottom-quark Yukawa couplings h_t and h_b . These effects could play a significant rôle not only in the effective Higgs potential [18] at the two-loop level, but may also affect directly the production of reconstructed polarized top and bottom quarks. We therefore generalize the discussion of CP-conserving vertex effects in the previous subsection of this report to include CP-violating vertex corrections. The Feynman diagrams shown in Fig. 12 induce the following CP-violating effective Lagrangian for the couplings:

$$-\mathcal{L}^{\text{eff}} = \left[(h_b + \delta h_b) \phi_1^{0*} + \Delta h_b \phi_2^{0*} \right] \bar{b}_R b_L + \left[(h_t + \delta h_t) \phi_2^0 + \Delta h_t \phi_1^0 \right] \bar{t}_R t_L + \text{h.c.}, \quad (3.23)$$

where

$$\begin{aligned} \frac{\delta h_b}{h_b} &\sim -\frac{2\alpha_s}{3\pi} \frac{m_{\tilde{g}}^* A_b}{\max(M_{\text{SUSY}}^2, |m_{\tilde{g}}|^2)} - \frac{|h_t|^2}{16\pi^2} \frac{|\mu|^2}{\max(M_{\text{SUSY}}^2, |\mu|^2)}, \\ \frac{\Delta h_b}{h_b} &\sim \frac{2\alpha_s}{3\pi} \frac{m_{\tilde{g}}^* \mu^*}{\max(M_{\text{SUSY}}^2, |m_{\tilde{g}}|^2)} + \frac{|h_t|^2}{16\pi^2} \frac{A_t^* \mu^*}{\max(M_{\text{SUSY}}^2, |\mu|^2)}, \end{aligned}$$

$$\begin{aligned}
\frac{\delta h_t}{h_t} &\sim -\frac{2\alpha_s}{3\pi} \frac{m_{\tilde{g}}^* A_t}{\max(M_{\text{SUSY}}^2, |m_{\tilde{g}}|^2)} - \frac{|h_b|^2}{16\pi^2} \frac{|\mu|^2}{\max(M_{\text{SUSY}}^2, |\mu|^2)}, \\
\frac{\Delta h_t}{h_t} &\sim \frac{2\alpha_s}{3\pi} \frac{m_{\tilde{g}}^* \mu^*}{\max(M_{\text{SUSY}}^2, |m_{\tilde{g}}|^2)} + \frac{|h_b|^2}{16\pi^2} \frac{A_b^* \mu^*}{\max(M_{\text{SUSY}}^2, |\mu|^2)},
\end{aligned} \tag{3.24}$$

and

$$\begin{aligned}
h_b &= \frac{g_w m_b}{\sqrt{2} M_W \cos \beta [1 + \delta h_b/h_b + (\Delta h_b/h_b) \tan \beta]}, \\
h_t &= \frac{g_w m_t}{\sqrt{2} M_W \sin \beta [1 + \delta h_t/h_t + (\Delta h_t/h_t) \cot \beta]}.
\end{aligned} \tag{3.25}$$

We see from these last relations that the modification of the Higgs-bottom Yukawa coupling is sizeable for large values of $\tan \beta$, whilst the corresponding corrections to the Higgs-top Yukawa coupling are less relevant.

3.4 CP Asymmetries

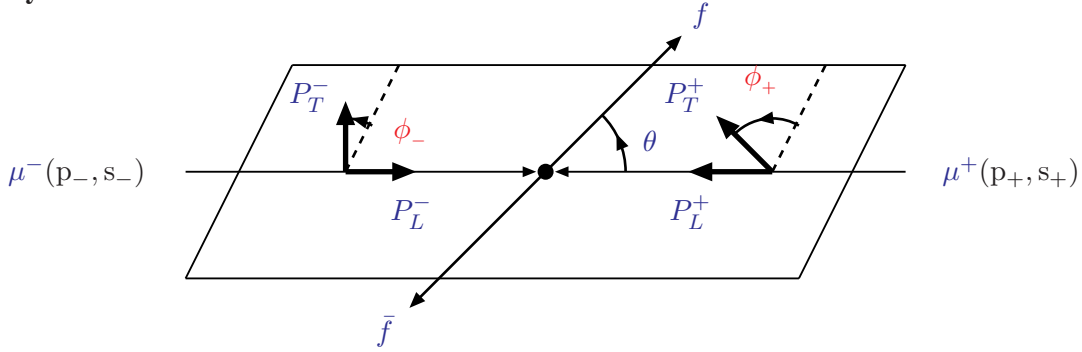


Fig. 13: CP asymmetries with polarized muons.

The possibility of muon polarization at a $\mu^+ \mu^-$ collider could play an essential role in unravelling the CP nature of the Higgs boson(s) and/or in probing CP violation in the Higgs sector. We display in Fig. 13 a general configuration of the polarizations of the initial muons. There are several CP-violating observables that can be constructed using muon polarization vectors and/or the three-momenta and spins of the final particles. For our illustrations, however, we concentrate on the following two representative CP-odd observables [53, 46]:

$$\mathcal{A}_{\text{CP}}^t = \frac{\sigma(\mu^-(s_x) \mu^+(s_y) \rightarrow f \bar{f}) - \sigma(\mu^-(s_x) \mu^+(-s_y) \rightarrow f \bar{f})}{\sigma(\mu^-(s_x) \mu^+(s_y) \rightarrow f \bar{f}) + \sigma(\mu^-(s_x) \mu^+(-s_y) \rightarrow f \bar{f})}, \tag{3.26}$$

$$\mathcal{A}_{\text{CP}}^l = \frac{\sigma(\mu^-(s_z) \mu^+(-s_z) \rightarrow f \bar{f}) - \sigma(\mu^-(-s_z) \mu^+(s_z) \rightarrow f \bar{f})}{\sigma(\mu^-(s_z) \mu^+(-s_z) \rightarrow f \bar{f}) + \sigma(\mu^-(-s_z) \mu^+(s_z) \rightarrow f \bar{f})}, \tag{3.27}$$

where $s_{x,y,z}$ are the x, y, z -projections of the spin s of the muon. Note that we define the positive z axis as the direction of the μ^- beam, and the y axis perpendicular to the earth surface pointing upwards to the sky. The CP-violating observable $\mathcal{A}_{\text{CP}}^t$ is even under naive CP'T' transformations, whereas $\mathcal{A}_{\text{CP}}^l$ is odd. To leading order, $\mathcal{A}_{\text{CP}}^t$ is generated by dispersive terms, whilst $\mathcal{A}_{\text{CP}}^l$ requires non-vanishing absorptive contributions.

The interactions of Higgs bosons H_i with mixed CP to fermions f are given by

$$\mathcal{L}_{\text{int}} = -\sum_{i=1}^3 H_i \frac{g_w m_f}{2M_W} \bar{f} \left(g_{H_i f f}^S + i g_{H_i f f}^P \right) f. \tag{3.28}$$

In the MSSM, the reduced scalar and pseudoscalar couplings $g_{H_i ff}^S$ and $g_{H_i ff}^P$ receive contributions from both self-energy and vertex corrections similar to those discussed previously in the CP-conserving case, and their analytic forms have been derived in [18]. Neglecting the γ , Z background, as appropriate at energies close to any Higgs-boson resonance $H_i : i = 1, 2, 3$, the CP-violating observable $\mathcal{A}_{\text{CP}}^t$ reads

$$\mathcal{A}_{\text{CP}}^t = \frac{2g_{H_i \mu\mu}^S g_{H_i \mu\mu}^P}{(g_{H_i \mu\mu}^S)^2 + (g_{H_i \mu\mu}^P)^2}. \quad (3.29)$$

We display in Fig. 14(a) the dependence of $\mathcal{A}_{\text{CP}}^t$ on $\arg(A_t)$ for the lightest Higgs boson H_1 , and Fig. 14(b) shows numerical estimates of $\mathcal{A}_{\text{CP}}^t$ for transversely-polarized up-type fermions. Correspondingly, numerical estimates related to the next-to-lightest H_2 boson are exhibited in Fig. 15.

The CP-violating observable $\mathcal{A}_{\text{CP}}^l$ defined by (3.27) may be approximated by [46]:

$$\mathcal{A}_{\text{CP}}^l \approx \frac{2\text{Re}(\hat{\Pi}^{HA}) \text{Im}(\hat{\Pi}^{AA} - \hat{\Pi}^{HH})}{(M_H^2 - M_A^2)^2 + (\text{Im} \hat{\Pi}^{AA})^2 + (\text{Im} \hat{\Pi}^{HH})^2}. \quad (3.30)$$

The expression (3.30) is derived under the assumption that only one CP-even Higgs boson H mixes actively with a CP-odd scalar A , after integrating out heavy degrees of freedom which amounts to a vanishing or rather suppressed $\text{Im} \hat{\Pi}^{HA}$ for energies below the TeV scale. Such a scenario has been studied in [46], within the context of a heavy-Majorana-neutrino model. We display in Fig. 16 numerical values for two scenarios with $M_A = 170$ and 400 GeV. In agreement with our earlier discussion, we observe that $\mathcal{A}_{\text{CP}}^l$ may become of order unity if $M_H - M_A \sim \Gamma_H, \Gamma_A$. As was discussed in [54] and is displayed in Fig. 17(c), (d) and (f), analogous features may be found in the MSSM with explicit radiative CP violation in the Higgs sector, where $\mathcal{A}_{\text{CP}}^t = \sigma_{\perp}/(\sigma_{LL} + \sigma_{RR})$ and $\mathcal{A}_{\text{CP}}^l = (\sigma_{LL} - \sigma_{RR})/(\sigma_{LL} + \sigma_{RR})$.

This pilot study indicates that the option of polarization for the μ^+ and μ^- beams may be very valuable for determining the CP nature of a Higgs boson and/or for analyzing a two-Higgs-boson-mixing system. However, the effective degree of polarization provided naturally in a $\mu^+\mu^-$ collider is currently not expected to be much larger than $P \sim 0.4$ for each beam [55]. Thus, the actual CP asymmetries must be reduced by a factor $P^2 \sim 1/10$ compared to the above predictions. Nevertheless, there may well be large observable effects. A complete evaluation of this opportunity requires further studies of both theoretical and experimental aspects, including background analyses originating from γ , Z -exchange graphs as well as the effects of polarization dilution.

3.5 Heavy Neutral Higgs-Boson Masses in the MSSM with Explicit CP Violation

We demonstrated earlier how resonant Higgs scalar-pseudoscalar transitions may lead to enhanced CP asymmetries at a $\mu^+\mu^-$ collider. We now explore an appealing theoretical framework for such studies, namely the MSSM with explicit radiative CP violation. In this case, the lightest neutral Higgs boson H_1 already offers interesting physics prospects. However, further opportunities are offered by the two heavier neutral Higgs bosons $H_{2,3}$, which are in general largely mixtures of the heavier ‘CP-even’ Higgs boson H and the ‘CP-odd’ pseudoscalar A , which can naturally have a mass splitting comparable to their widths [45, 18]. This mass splitting will in general be increased by scalar-pseudoscalar mixing (3.22), as seen in Fig. 18. This figure contrasts recent results found for pole masses of $H_{2,3}$ [47] using the code `cph+.f` [56] with previous results found in an effective-potential approach [18]. We see that these calculations are significantly different, in particular for larger values of the charged Higgs-boson mass, m_{H^+} , and in the vicinity of the stop threshold.

The results are plotted as functions of $\text{Arg}(A_t)$, the CP-violating phase of A_t . We see that the difference in masses between the two heavier neutral Higgs bosons may easily be increased by a large factor if $\text{Arg}(A_t)$ is large.

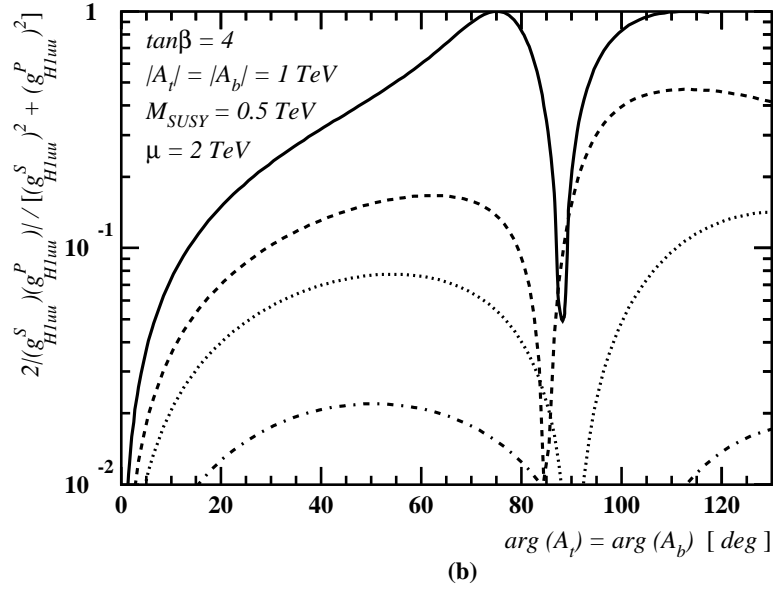
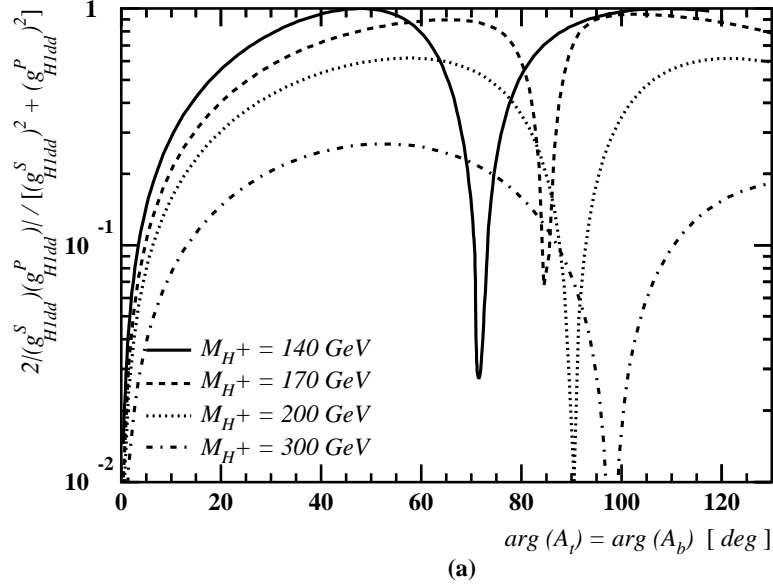


Fig. 14: Numerical estimates of (a) $2|(g_{H_1 dd}^S)(g_{H_1 dd}^P)|/[(g_{H_1 dd}^S)^2 + (g_{H_1 dd}^P)^2]$ and (b) $2|(g_{H_1 uu}^S)(g_{H_1 uu}^P)|/[(g_{H_1 uu}^S)^2 + (g_{H_1 uu}^P)^2]$ as functions of $\arg(A_t)$.

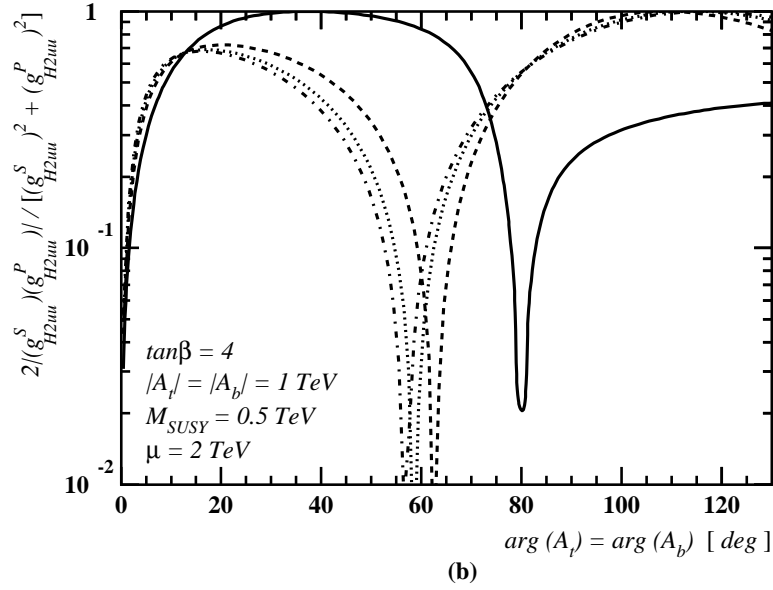
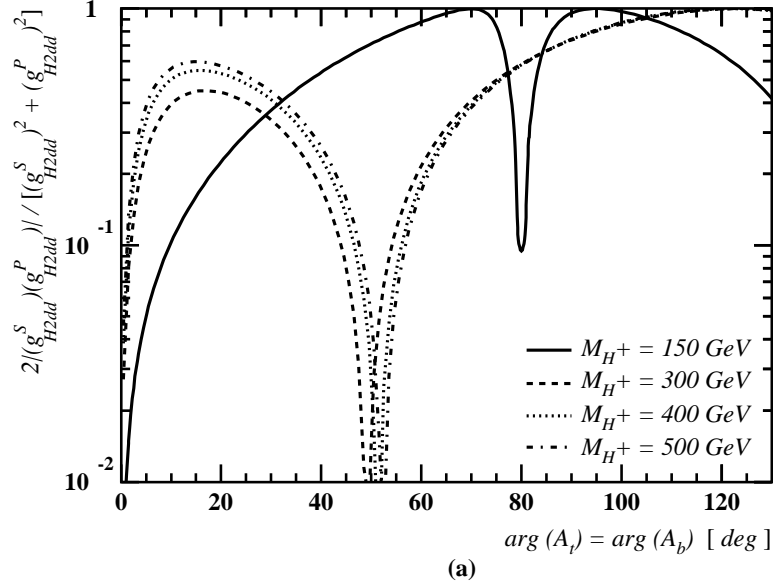


Fig. 15: Numerical estimates of (a) $2|(g_{H_2dd}^S)(g_{H_2dd}^P)|/[(g_{H_2dd}^S)^2 + (g_{H_2dd}^P)^2]$ and (b) $2|(g_{H_2uu}^S)(g_{H_2uu}^P)|/[(g_{H_2uu}^S)^2 + (g_{H_2uu}^P)^2]$ as functions of $\arg(A_t)$.

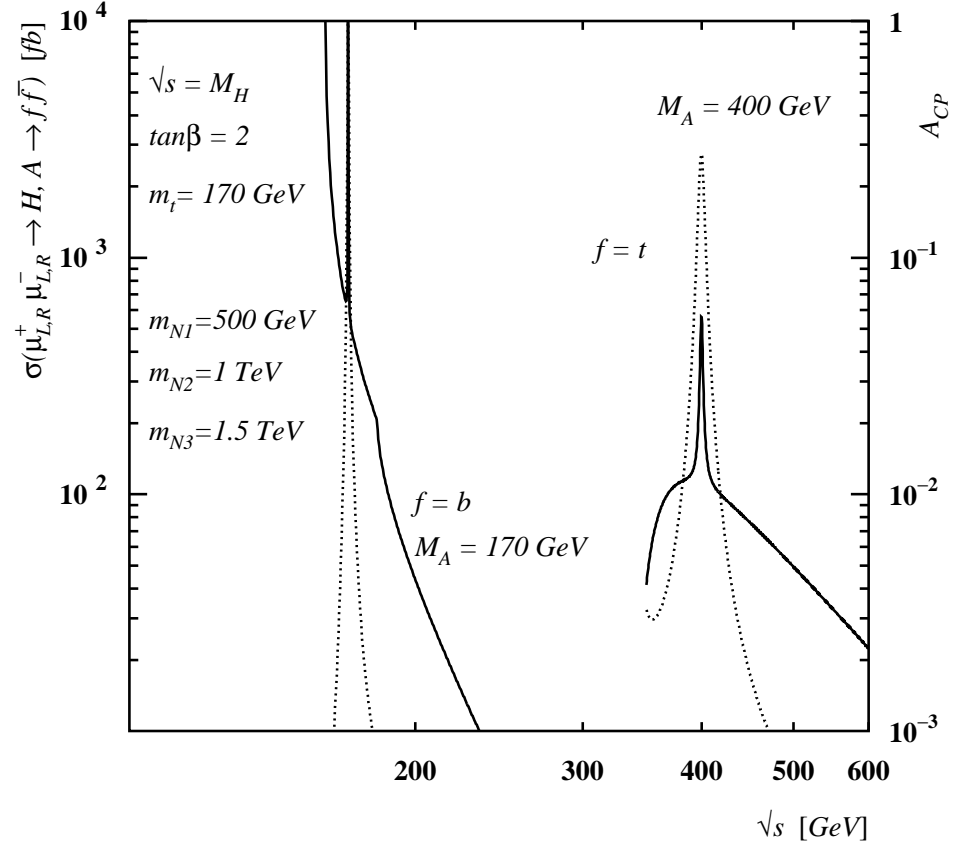


Fig. 16: Numerical values for the cross section (solid lines) and \mathcal{A}_{CP}^l (dashed lines) as functions of the cms energy \sqrt{s} , for an E_6 -inspired model with heavy Majorana neutrinos [46].

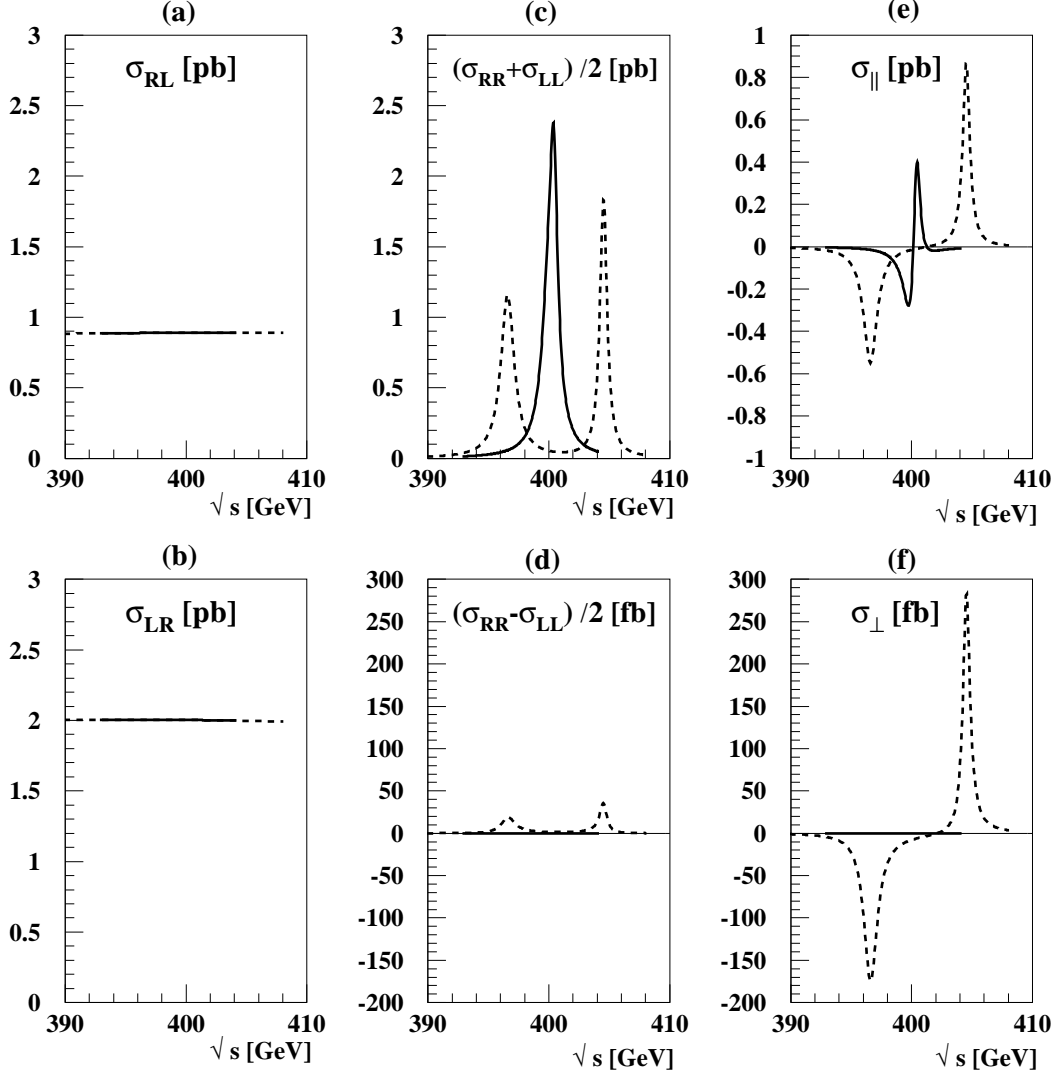


Fig. 17: The dependence of polarized-muon cross sections on the centre-of-mass energy \sqrt{s} , as estimated in [54] for the MSSM with explicit CP violation. The selected parameters are: $\tan\beta = 3$, $M_{H^+} \approx 0.4$ TeV, $M_{\text{SUSY}} = 0.5$ TeV, $|A_{t,b}| = |\mu| = 1$ TeV and $\arg(\mu A_t) = 0$ (solid lines) and 90° (dashed lines).

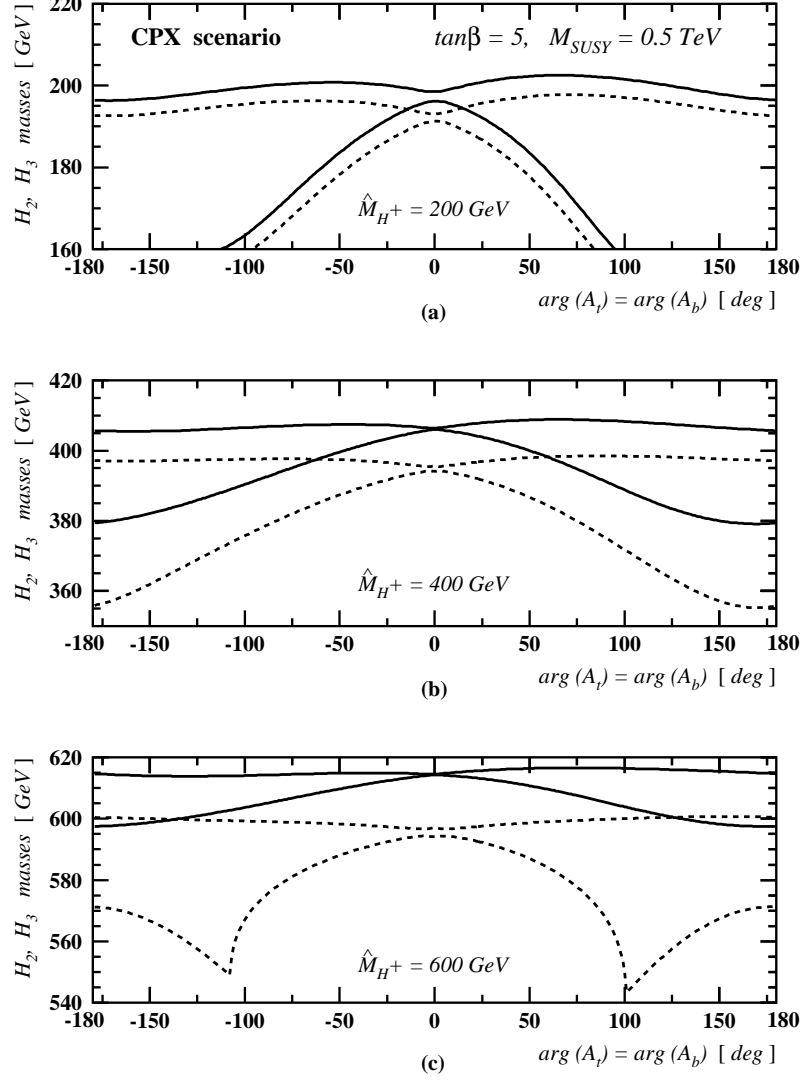


Fig. 18: Numerical values for the mass splitting between the second and third neutral Higgs bosons $H_{2,3}$ of the MSSM, as functions of $\text{Arg}(A_t)$, the CP-violating phase of A_t , for the indicated values of the other MSSM parameters. There are significant differences between the mass differences calculated in the effective-potential approximation (solid lines) and using the pole masses. We note that the mass splitting may be increased by a large factor for large values of $\text{Arg}(A_t)$ [18].

The detailed study of CP-violating observables as a function of the centre-of-mass energy across the double $H_{2,3}$ peak is left for another occasion, but it is clear that the beam polarization discussed earlier would be a valuable tool, as well as studies of the polarization states of $H_{2,3}$ decay products.

4 Precise Determination of the Higgs–Chargino Couplings in Chargino-Pair Production

We now give one example of the interesting CP-conserving physics accessible at a second $\mu^+\mu^-(H, A)$ factory: chargino-pair production at such a $\mu^+\mu^-$ collider offers an outstanding possibility for the precise determination of the Higgs-chargino couplings. Within the framework of the MSSM, decays of the heavy neutral Higgs bosons H, A into two light charginos can be observed with significant branching ratios in certain parameter regions. Fig. 19 shows branching ratios up to 50 % in mixed scenarios with $|\mu| \sim M_2$ for $\tan \beta = 5$ and $m_A = 350$ GeV, assuming CP symmetry⁵. We study the pair production of light charginos with mass $m_{\tilde{\chi}_1^\pm} = 155$ GeV in such a mixed scenario with $M_2 = -\mu = 188$ GeV, and in a scenario with a gaugino-dominated light chargino: $M_2 = 155$ GeV, $\mu = -400$ GeV for comparison.

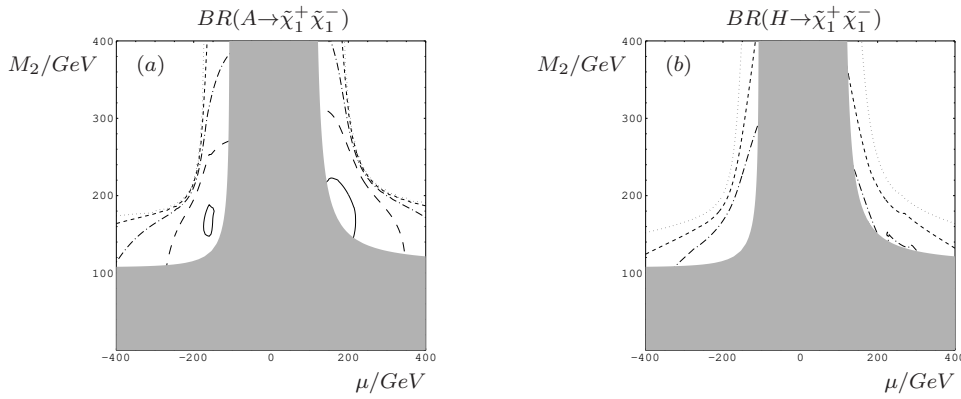


Fig. 19: Branching ratios of the heavy Higgs bosons A and H into light-chargino pairs for $m_A = 350$ GeV and $\tan \beta = 5$, computed with the program HDECAY [57]. The contour lines correspond to 0.1 (dotted), 0.2 (dashed), 0.3 (dash-dotted), 0.4 (large dashed) and 0.5 (continuous). The gray area is the experimentally excluded region.

The cross section for chargino-pair production, $\mu^+\mu^- \rightarrow \tilde{\chi}_1^+\tilde{\chi}_1^-$, around the H and A Higgs resonances with no energy spread and a finite energy resolution $R = 0.06\%$, is shown in Fig. 20. Since the energy separation between the resonances is in this case larger than their widths and the energy spread, the two Higgs resonances can be separated clearly. Since we assume here CP conservation, the H resonance is P-wave suppressed by the factor $(1 - 4m_{\tilde{\chi}_1^\pm}^2/s)$. The peak of the A resonance is thus higher than the H peak in both scenarios, although chargino couplings to H are larger. Comparing the scenarios, the A resonance is lower in the mixed scenario despite larger couplings and branching ratios, since also the A decay width becomes larger, because of decay channels into neutralinos.

The ratio of the Higgs-chargino couplings

$$x := \frac{c_{H\tilde{\chi}_1^+\tilde{\chi}_1^-}^2}{c_{A\tilde{\chi}_1^+\tilde{\chi}_1^-}^2} \quad (4.31)$$

⁵There are interesting additional physics opportunities in chargino production and decay in the MSSM with CP violation, extending the analysis of the previous section, which we leave for a future occasion.

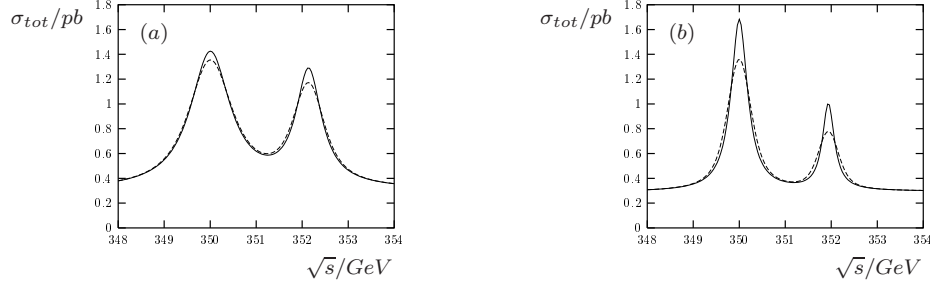


Fig. 20: The total cross section σ_{tot} for $\mu^+\mu^- \rightarrow \tilde{\chi}_1^+\tilde{\chi}_1^-$ in (a) the mixed and (b) the gaugino scenarios, for $m_{\tilde{\nu}_\mu} = 261$ GeV, with no energy spread (continuous) and with a finite energy resolution $R = 0.06\%$ (dashed).

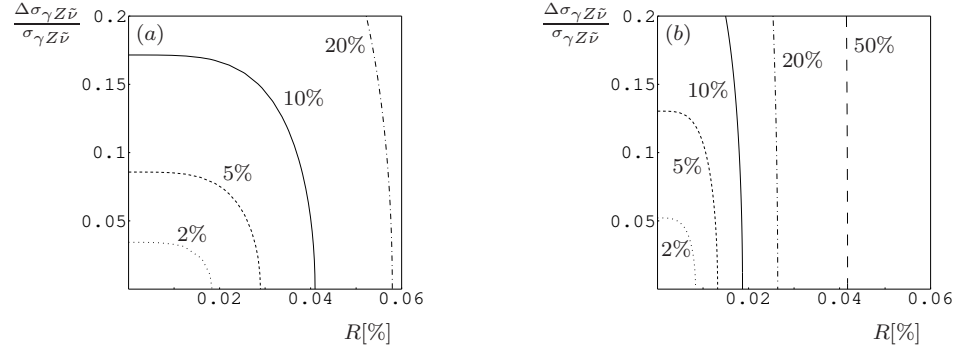


Fig. 21: Relative error in the ratio of the Higgs-chargino couplings x as a function of the energy resolution and the relative error in the non-Higgs channels, in (a) the mixed and (b) the gaugino scenarios.

can be determined by measuring the ratio of the cross sections on the Higgs resonance peaks: [58]

$$r = \frac{\sigma_H(m_H) + \sigma_A(m_H)}{\sigma_H(m_A) + \sigma_A(m_A)} = \frac{\sigma_{tot}(m_H) - \sigma_{\gamma Z \tilde{\nu}}(m_H)}{\sigma_{tot}(m_A) - \sigma_{\gamma Z \tilde{\nu}}(m_A)}, \quad (4.32)$$

where $\sigma_H(m_{H,A})$, $\sigma_A(m_{H,A})$ and $\sigma_{\gamma Z \tilde{\nu}}(m_{H,A})$ are the contributions to the chargino-pair production cross section from H exchange, A exchange and $\gamma/Z/\tilde{\nu}$ exchanges at the top of the H , A resonances, respectively, neglecting the contribution of the lightest Higgs scalar h . Interference between the two Higgs-boson exchange channels vanishes when CP is conserved, as we assume here. It would be interesting to study the same reaction in the MSSM with explicit loop-induced CP violation, along the lines discussed in the previous section. Interferences between the Higgs channels and the non-Higgs channels are of order $\mathcal{O}(m_\mu/\sqrt{s})$, and are therefore neglected.

We note that the ratio r , and therefore also x , is independent of the chargino decay characteristics. Then the error in the determination of the Higgs-chargino couplings plotted in Fig. 21 depends on the energy resolution of the muon beams and on the error in the measurement of the non-Higgs contributions at the Higgs resonances in r , that can be estimated, e.g., from cross-section measurements off the resonances. The effect of the energy resolution on the cross sections and widths is larger if the widths are narrower. With an energy resolution of $R = 0.04\%$, the relative error on x in the mixed scenario is larger than 10%, whereas in the gaugino scenario it lies around 50%. If, on the other hand, values of $R \sim 0.01\%$ are achieved, the error induced is in both cases of the order of 1%. With knowledge of the energy spread, the errors in the widths and cross sections can be substantially reduced [7]. A detailed analysis of chargino and neutralino production at a $\mu^+\mu^-$ collider and the precise determination of the Higgs couplings will be given in [58].

We conclude that chargino production via s -channel Higgs exchange at a $\mu^+\mu^-$ collider may allow a precise determination of the Higgs-chargino couplings in the MSSM, if the resonances can be separated. We leave for a future occasion discussions of the cases where the resonances overlap, and when CP violation is important.

5 Conclusions

We have seen in this chapter some of the physics opportunities offered by $\mu^+\mu^-$ colliders operated as Higgs factories. Interest in these opportunities has been stimulated by the possible existence of a light Higgs boson. The case outlined here depends indeed upon the mass of this lightest Higgs boson, and, although all the indications are favourable, this remains an unknown parameter.

A first muon collider (FMC) operating around the peak of the Standard Model (SM) Higgs boson, that is expected to weigh ~ 120 GeV, as seen in Fig. 1, offers interesting prospects for precision measurements of properties of the SM Higgs boson, such as its mass and decay width. The mass could be measured to an unprecedented accuracy in the sub-MeV region. A direct width determination would be possible to an accuracy of $\mathcal{O}(1)$ MeV. By varying judiciously the beam-energy spread, an interesting peak event rate could be attained for a SM Higgs mass up to about 160 GeV, and measurements of decays into $b\bar{b}$, $\tau^+\tau^-$ and WW^* may be possible. The accuracies obtained for these branching ratios are in the same ball park as those expected at an e^+e^- linear collider (LC). However, they are highly dependent on the available luminosity and the details of the detector, which are not yet fixed for the FMC. Notice also that by combining with LC measurements the coupling of the Higgs boson to $\mu^+\mu^-$ could be determined with an accuracy of $\sim 4\%$ at the FMC [8].

If supersymmetry plays a rôle at the electroweak scale, one expects a richer Higgs sector, containing three neutral Higgs bosons h, H, A . As we have shown, the production cross sections and branching ratios of h, H, A are very sensitive to supersymmetric radiative corrections. As we have also shown, polarized $\mu^+\mu^-$ beams would offer in addition interesting opportunities to explore CP violation in decay vertices and/or Higgs-mass mixing. The masses of H, A may already be estimated quite accurately using FMC measurements. A second Higgs factory (SMC) tuned to the twin H, A peaks offers valuable prospects for measuring the two masses independently (due to the fine energy resolution reachable at a $\mu^+\mu^-$ collider), the couplings of the heavy Higgs bosons to SM and supersymmetric particles, as well as the opportunity for further interesting measurements of possible CP violation in the MSSM Higgs sector.

We have not discussed in this report the physics prospects offered by a high-energy $\mu^+\mu^-$ collider. As is well known, this would have certain advantages over a high-energy e^+e^- collider, notably in the beam energy spread and in the accuracy with which the beam energy could be calibrated using the precession of the μ^\pm polarization. However, it is too early to know whether these advantages would be conclusive, and a multi-TeV $\mu^+\mu^-$ collider would presumably need to be preceded by one or more lower-energy Higgs factories.

Acknowledgements

S.K. thanks the CERN Theory Division for financial support during a stay at CERN. The work of D.G. is supported by the European Commission TMR programme under the grant ERBFMBICT 983539.

References

- [1] M. Carena, J. Conway, H. Haber and J. Hobbs, *et al.*, *Report of the Tevatron Higgs Working Group*, hep-ph/0010338.

- [2] ATLAS Collaboration, *Detector and Physics Performance Technical Design Report*, CERN/LHCC/99-15 (1999), see: <http://atlasinfo.cern.ch/Atlas/GROUPS/PHYSICS/TDR/access.html>; CMS Collaboration, see: <http://cmsinfo.cern.ch/Welcome.html/CMSdocuments/CMSplots/>.
- [3] TESLA TDR Part 3: “Physics at an e^+e^- Linear Collider”, eds. R.D. Heuer, D. Miller, F. Richard and P.M. Zerwas, hep-ph/0106315, see: <http://tesla.desy.de>.
- [4] T. Abe *et al.* [American Linear Collider Working Group Collaboration], *Resource book for Snowmass 2001*, hep-ex/0106055, hep-ex/0106056, hep-ex/0106057, hep-ex/0106058.
- [5] K. Abe *et al.* [ACFA Linear Collider Working Group Collaboration], hep-ph/0109166.
- [6] Proceedings of the Workshop on Physics at the First Muon Collider and at the front end of the Muon Collider, eds. S. Geer and R. Raja, 6-9 Nov 1997, Batavia, Illinois, USA (AIP Conf. Proc. 435); see also http://www.fnal.gov/projects/muon_collider/
- [7] B. Autin *et al.*, Prospective study of muon storage rings at CERN, CERN 99-02, ECFA 99-197 (1999).
- [8] V. D. Barger, M. Berger, J. F. Gunion and T. Han, in *Proc. of the APS/DPF/DPB Summer Study on the Future of Particle Physics (Snowmass 2001)*, eds. R. Davidson and C. Quigg, hep-ph/0110340.
- [9] LEP Electro-weak working group, <http://lepewwg.web.cern.ch/LEPEWWG/>; U. Baur *et al.*, hep-ph/0111314.
- [10] A. D. Martin, J. Outhwaite and M. G. Ryskin, Phys. Lett. B **492** (2000) 69.
- [11] The ALEPH, DELPHI, L3 and OPAL Collaborations, and the LEP Higgs Working Group, hep-ex/0107029.
- [12] J. Erler, Phys. Rev. D **63** (2001) 071301.
- [13] C. Tully, talk at the 18th International Workshop on Weak Interactions and Neutrinos, 21-26 Jan 2002, Christchurch, New Zealand.
- [14] H. Haber and R. Hempfling, Phys. Rev. Lett. **66** (1991) 1815; M. Carena, M. Quirós and C.E.M. Wagner, Nucl. Phys. B **461** (1996) 407; H. Haber, R. Hempfling and A. Hoang, Z. Phys. C **75** (1997) 539; S. Heinemeyer, W. Hollik and G. Weiglein, Phys. Rev. D **58** (1998) 091701 and Eur. Phys. J. C **9** (1999) 343; R.-J. Zhang, Phys. Lett. B **447** (1999) 89.
- [15] J. Ellis, S. Heinemeyer, K. Olive and G. Weiglein, Phys. Lett. B **515** (2001) 348.
- [16] C. Ankenbrandt *et al.*, Status of Muon Collider Research and Development and Future Plans, Phys. Rev. ST Accel Beams **2**, 081001.
- [17] J. R. Ellis and D. Ross, Phys. Lett. B **506** (2001) 331.
- [18] M. Carena, J. Ellis, A. Pilaftsis and C.E.M. Wagner, Nucl. Phys. B **586** (2000) 92.
- [19] V. D. Barger, M. S. Berger, J. F. Gunion and T. Han, Phys. Rept. **286** (1997) 1; M. S. Berger, Phys. Rev. Lett. **87** (2001) 131801.
- [20] R. Casalbuoni, A. Deandrea, S. De Curtis, D. Dominici, R. Gatto, J. F. Gunion, Phys. Rev. Lett. **83** (1999).
- [21] DELPHI collaboration, P. Abreu *et al.*, Phys. Lett. B **397** (1997) 158.

- [22] J. Guasch, W. Hollik and S. Peñaranda, Phys. Lett. B **515** (2001) 367.
- [23] V. D. Barger, T. Han and C. G. Zhou, Phys. Lett. B **480** (2000) 140.
- [24] S. Heinemeyer, W. Hollik and G. Weiglein, Eur. Phys. Jour. C **16** (2000) 139.
- [25] M. Carena, S. Mrenna and C.E.M. Wagner, Phys. Rev. D **60** (1999) 075010; Phys. Rev. D **62** (2000) 055008.
- [26] W. Loinaz and J. D. Wells, Phys. Lett. B **445** (1998) 178.
- [27] S. Heinemeyer and G. Weiglein, in preparation.
- [28] S. Heinemeyer, W. Hollik and G. Weiglein, Comp. Phys. Comm. **124** (2000) 76; hep-ph/0002213; see <http://www.feynhiggs.de>.
- [29] The ALEPH, DELPHI, L3 and OPAL Collaborations, and the LEP Higgs Working Group, hep-ex/0107030.
- [30] J. Ellis, S. Heinemeyer, K. Olive and G. Weiglein, in preparation.
- [31] CLEO Collaboration, M. S. Alam *et al.*, Phys. Rev. Lett. **74** (1995) 2885 as updated in S. Ahmed *et al.*, CLEO CONF 99-10; K. Abe *et al.*, Belle Collaboration, hep-ex/0103042;
- [32] G. Degrossi, P. Gambino and G. F. Giudice, JHEP **0012** (2000) 009; see also M. Carena, D. Garcia, U. Nierste and C.E.M. Wagner, Phys. Lett. B **499** (2001) 141.
- [33] H. N. Brown *et al.*, Muon $g_\mu - 2$ Collaboration, Phys. Rev. Lett. **86** (2001) 2227; A. Czarnecki and W. J. Marciano, Phys. Rev. D **64** (2001) 013014. We take into account the sign correction pointed out by M. Knecht and A. Nyffeler, hep-ph/0111058; M. Knecht, A. Nyffeler, M. Perrottet and E. De Rafael, hep-ph/0111059.
- [34] J. Ellis, J.S. Hagelin, D.V. Nanopoulos, K.A. Olive and M. Srednicki, Nucl. Phys. B **238** (1984) 453; see also H. Goldberg, Phys. Rev. Lett. **50** (1983) 1419.
- [35] B. Ananthanarayan, G. Lazarides and Q. Shafi, Phys. Rev. D **44** (1991) 1613; T. Banks, Nucl. Phys. B **303** (1988) 172; M. Olechowski and S. Pokorski, Phys. Lett. B **214** (1988) 393; S. Dimopoulos, L.J. Hall and S. Raby, Phys. Rev. Lett. **68** (1992) 1984 and Phys. Rev. D **45** (1992) 4192; G.W. Anderson, S. Raby, S. Dimopoulos and L.J. Hall, Phys. Rev. D **47** (1993) 3702; R. Hempfling, Phys. Rev. D **49** (1994) 6168;
- [36] L.J. Hall, R. Rattazzi and U. Sarid, Phys. Rev. D **50** (1994) 7048; M. Carena, M. Olechowski, S. Pokorski and C.E.M. Wagner, Nucl. Phys. B **426** (1994) 269.
- [37] M. Carena, D. Garcia, U. Nierste and C.E.M. Wagner, Nucl. Phys. B **577** (2000) 88.
- [38] J. F. Gunion, H. E. Haber, G. L. Kane and S. Dawson, *The Higgs Hunter's Guide*, Addison-Wesley (1990).
- [39] H. Haber, M. Herrero, H. Logan, S. Penaranda, S. Rigolin and D. Temes, Phys. Rev. D **63** (2001) 055004.
- [40] H. Eberl, K. Hidaka, S. Kraml, W. Majerotto, Y. Yamada, Phys. Rev. D **62** (2000) 055006.
- [41] T.D. Lee, Phys. Rev. D **8** (1973) 1226.
- [42] S. Weinberg, Phys. Rev. Lett. **37** (1976) 657; G.C. Branco, Phys. Rev. Lett. **44** (1980) 504.
- [43] H. Georgi and G. Pais, Phys. Rev. D **10** (1974) 1246.

- [44] J.C. Romao, Phys. Lett. B **173** (1986) 309.
- [45] A. Pilaftsis, Phys. Rev. D **58** (1998) 096010 and Phys. Lett. B **435** (1998) 88; A. Pilaftsis and C.E.M. Wagner, Nucl. Phys. B **553** (1999) 3; D.A. Demir, Phys. Rev. D **60**(1999) 055006; S.Y. Choi, M. Drees and J.S. Lee, Phys. Lett. B **481** (2000) 57; S. Heinemeyer, Eur. Phys. J. C **22** (2001) 521.
- [46] A. Pilaftsis, Phys. Rev. Lett. **77** (1996) 4996; Nucl. Phys. B **504** (1997) 61.
- [47] M. Carena, J. Ellis, A. Pilaftsis, C.E.M. Wagner, Nucl. Phys. B **625** (2002) 345.
- [48] J. Papavassiliou and A. Pilaftsis, Phys. Rev. Lett. **75** (1995) 3060; Phys. Rev. D **53** (1996) 2128; Phys. Rev. D **54** (1996) 5315; Phys. Rev. Lett. **80** (1998) 2785; Phys. Rev. D **58** (1998) 053002.
- [49] For discussions that include EDM constraints from ^{199}Hg , see T. Falk, K. A. Olive, M. Pospelov and R. Roiban, Nucl. Phys. B **560** (1999) 3; S. Abel, S. Khalil and O. Lebedev, Nucl. Phys. B **606** (2001) 151.
- [50] J. Ellis and R. A. Flores, Phys. Lett. B **377** (1996) 83; A. Bartl, T. Gajdosik, W. Porod, P. Stockinger and H. Stremnitzer, Phys. Rev. D **60** (1999) 073003.
- [51] T. Ibrahim and P. Nath, Phys. Lett. B **418** (1998) 98; Phys. Rev. D **58** (1998) 111301; M. Brhlik, L. Everett, G. L. Kane and J. Lykken, Phys. Rev. Lett. **83** (1999) 2124.
- [52] For two-loop EDM constraints on A_t , see D. Chang, W.-Y. Keung and A. Pilaftsis, Phys. Rev. Lett. **82** (1999) 900; A. Pilaftsis, Phys. Lett. B **471** (1999) 174; D. Chang, W.-F. Chang and W.-Y. Keung, Phys. Lett. B **478** (2000) 239.
- [53] B. Grzadkowski and J. F. Gunion, Phys. Lett. B **350**(1995) 218; D. Atwood and A. Soni, Phys. Rev. D **52** (1995) 6271.
- [54] E. Asakawa, S. Y. Choi and J. S. Lee, Phys. Rev. D **62** (2000) 115005.
- [55] B. Grzadkowski, J. F. Gunion and J. Pliszka, Nucl. Phys. B **583** (2000) 49.
- [56] The Fortran code `cph+.f` is available from <http://pilaftsi.home.cern.ch/pilaftsi>.
- [57] A. Djouadi, J. Kalinowski and M. Spira, Comput. Phys. Commun. **108** (1998) 56.
- [58] H. Fraas, F. Franke, F. von der Pahlen, in preparation.